(2)

AD_____

CONTRACT NO: DAMD17-88-C-8125

TITLE: SPECTROSCOPY OF BURN WOUNDS

PRINCIPAL INVESTIGATORS: Martin A. Afromowitz, Ph.D.
James D. Callis, Ph.D.

CONTRACTING ORGANIZATION: University of Washington
Department of Electrical Engineering
and Department of Chemistry
Seattle, WA 98195

REPORT DATE: November 19, 1990

TYPE OF REPORT: Annual Report

PREPARED FOR: U.S. ARMY MEDICAL RESEARCH AND DEVELOPMENT COMMAND
Fort Detrick, Frederick, Maryland 21702-5012

SECURITY CLASSIFICATION OF THIS PAGE

REPORT DOCUMENTATION PAGE

Form Approved
OMB No. 0704-0188

1a. REPORT SECURITY CLASSIFICATION Unclassified	1b. RESTRICTIVE MARKINGS
2a. SECURITY CLASSIFICATION AUTHORITY	3. DISTRIBUTION / AVAILABILITY OF REPORT Approved for public release; distribution unlimited
2b. DECLASSIFICATION / DOWNGRADING SCHEDULE	
4. PERFORMING ORGANIZATION REPORT NUMBER(S)	5. MONITORING ORGANIZATION REPORT NUMBER(S)
6a. NAME OF PERFORMING ORGANIZATION University of Washington 6b. OFFICE SYMBOL (If applicable)	7a. NAME OF MONITORING ORGANIZATION
6c. ADDRESS (City, State, and ZIP Code) Department of Electrical Engineering and Department of Chemistry Seattle, WA 98195	7b. ADDRESS (City, State, and ZIP Code)
8a. NAME OF FUNDING / SPONSORING ORGANIZATION U.S. Army Medical Research & Development Command 8b. OFFICE SYMBOL (If applicable)	9. PROCUREMENT INSTRUMENT IDENTIFICATION NUMBER Contract No. DAMD17-88-C-8125
8c. ADDRESS (City, State, and ZIP Code) Fort Detrick Frederick, Maryland 21702-5012	10. SOURCE OF FUNDING NUMBERS PROGRAM ELEMENT NO. 63002A; PROJECT NO. 3M2 63002D840; TASK NO. DA; WORK UNIT ACCESSION NO. 001

11. TITLE (Include Security Classification)

SPECTROSCOPY OF BURN WOUNDS

12. PERSONAL AUTHOR(S)

Martin A. Afromowitz, Ph.D., James D. Callis, Ph.D.

13a. TYPE OF REPORT	13b. TIME COVERED	14. DATE OF REPORT (Year, Month, Day)	15. PAGE COUNT
Annual Report	FROM 7/15/89 TO 7/14/90	1990 November 1990	69

16. SUPPLEMENTARY NOTATION

17. COSATI CODES			18. SUBJECT TERMS (Continue on reverse if necessary and identify by block number)
FIELD	GROUP	SUB-GROUP	RA II; Volunteers; Diagnosis; Burn Wounds; Burn Depth; Instrument
06	05		
06	12		

19. ABSTRACT (Continue on reverse if necessary and identify by block number)

This research seeks to develop non-invasive burn depth evaluation from non-contacting visible and near-infrared spectroscopic measurements. In previous years, we demonstrated that features of the optical reflection spectra of burn wounds can be correlated with the depth or burn. An imaging system was built which determined, with accuracy equal to or better than that of a skilled burn surgeon, the probability that burn sites would heal within three weeks from date of injury. Our goal for the current project is to investigate the optical reflectance properties of burns, utilizing the techniques of multivariate analysis, in order to improve the reliability of this instrument and to develop methods which will permit detailed monitoring of the healing process. (continued)

20. DISTRIBUTION / AVAILABILITY OF ABSTRACT ☐ UNCLASSIFIED/UNLIMITED ☐ SAME AS RPT ☐ DTIC USERS	21. ABSTRACT SECURITY CLASSIFICATION Unclassified
22a. NAME OF RESPONSIBLE INDIVIDUAL Mrs. Virginia M. Miller	22b. TELEPHONE (Include Area Code) (301) 663-7325 22c. OFFICE SYMBOL SGRD-RMI-S

DD Form 1473, JUN 86 *Previous editions are obsolete.* SECURITY CLASSIFICATION OF THIS PAGE

19. ABSTRACT (Continued)

Excellent progress has been made toward achievement of the goals of this project. Last year a commercial spectrophotometer (LT Quantum 1200) was purchased and was modified to make optical reflection measurements in both the visible and near-infrared regions (450-1800 nm). A library of reference spectra was acquired with this instrument.[1]

This year, considerable progress has been made in understanding the major components of the reflectance spectra of human skin *in vivo*. Three dynamic processes which influence *in vivo* spectra have been studied to improve our knowledge of burn physiology: 1) temperature, 2) ischemia, and 3) inflammation and healing in a shallow burn. The near-infrared spectrum of human tissue is dominated by water. We have mathematically analyzed spectra of pure water for the purpose of compensating for water absorbances in tissues in order to study other components of tissue. Vasodilation and ischemia have been modeled in healthy human subjects and have been observed in the healing of a minor burn.

Excellent progress has been made towards improving predictions of burn healing potential. Twenty-five patients at Harborview Burn Center were studied, and the visible reflectance spectra of their burns were analyzed. An unexpected absorption band was observed at 630 nm which correlated to burn depth. It was identified as methemoglobin. Multivariate statistics led to a new spectral model which predicted the healing potential of 66 burn sites with 98% accuracy, significantly better than the surgeons' predictions (88%). This model suggests that the ratio of methemoglobin to oxyhemoglobin is indicative of burn depth.

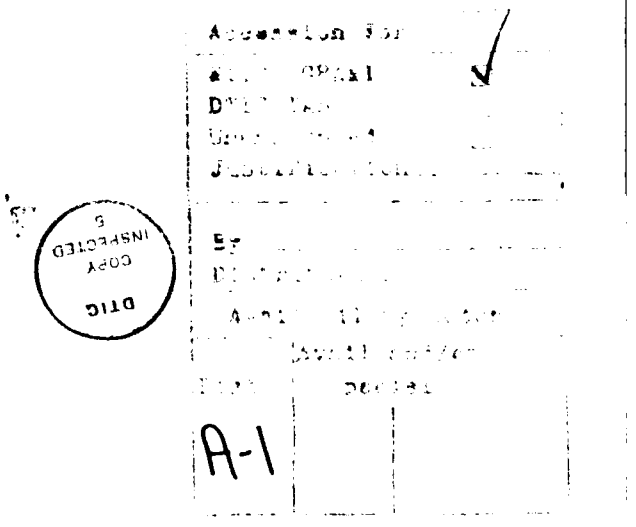

FOREWORD

Opinions, interpretations, conclusions and recommendations are those of the author and are not necessarily endorsed by the U.S. Army.

____ Where copyrighted material is quoted, permission has been obtained to use such material.

____ Where material from documents designated for limited distribution is quoted, permission has been obtained to use the material.

N/A Citations of commercial organizations and trade names in this report do not constitute an official Department of the Army endorsement or approval of the products or services of these organizations.

____ In conducting research using animals, the investigator(s) adhered to the "Guide for the Care and Use of Laboratory Animals," prepared by the Committee on Care and Use of Laboratory Animals of the Institute of Laboratory Animal Resources, National Research Council (NIH Puolication No. 86-23, Revised 1985).

N/A For the protection of human subjects, the investigator(s) have adhered to policies of applicable Federal Law 45CFR46.

Walter D. Sizemore May 22, 1991

PI Signature Date

I. Fundamental Studies of Water.

Introduction. In order to understand the real factors that lead to the changes in reflection spectra from the burn sites, we have to investigate the temperature dependence of the water combination tones peaks in the wavelength range used in our *in vivo* studies of human tissue. The main goal of these studies is to understand the structure of the observed peaks and the kinetics of the real molecules and structures that causes the observed changes in spectra. Another problem arises from the nonlinear dependence of the reflection spectra on the extinction and scattering of the tissue. In order to build a realistic model for temperature dependent reflection spectra, we need to find the "pure components" of the spectra and their behavior upon change of temperature. As long as water is the dominant component of tissue, understanding the structure of water and specificaliy how hydrogen bonding affects NIR spectra is one of the prominent problems in biophysics.

The structure of liquid water remains a most puzzling problem in the chemistry of solutions and electrolytes. Despite numerous attempts to build a consistent model of water through empirical data collected over the last 60 years, it must be admitted that no single description satisfactorily explains the majority of the collected data.[2] In principle, vibrational spectroscopy provides a precise tool for elucidation of the various species existing in water and water solutions. However, even in such a straightforward endeavor as deriving thermodynamic properties from IR absorbtion spectrophotometry and Raman-spectroscopy, the results are in poor agreement with each other and with other methods such as calorimetry. The main source of this ambiguity in spectra interpretation is concerned with the problems of the baseline determination[3] and with the difficulty of interpolation and deconvolution of broad bands which undergo subtle changes. A number of investigators have attempted to deconvolve the absorption bands into an arbitrary number of gaussian bands. There is no theoretical reason for this procedure and the results are not consistent with any known theory. Recent advances in short wavelength NIR spectroscopy, driven by new technology for multichannel silicon

detectors, makes this region of the water spectra, where only overtone and combination bands exist, very attractive for investigation. Indeed, many models of water explaining different features of the SW-NIR exist in the literature.[4-12] The first studies of NIR combination bands were done more than three decades ago by Suhrmann and Breyer.[4,5] More recent investigation of NIR bands and a suggestion of a model containing three water species have been described by G.R.Choppin and K.Buijs in the early 60's.[7-8] They proposed that three bands can be distinguished in the absorption band of water between 1100 and 1300 nm, giving the spectral assignments and the extinction coefficients for each band. The concentration of each of the three absorbing species was calculated as a function of water temperature. Using this model and the concentration of each species, a number of the properties of water were calculated. The species were assumed to be nonbonded(monomer) and hydrogen bonded (dimer and trimer) intramolecular complexes. Their enthalpies were calculated from Van't Hoff equilibrium equations. Subsequently, different authors proposed models of water with two[8] and even five species[8] and many theoretical papers examining different models appeared in the last three decades. The most popular is the model proposed by Choppin and Buijis, and later elaborated by Senior and Vand[10], that explains the spectroscopic data in terms of bonded and nonbonded groups of molecules in water, is referred to as a mixture model. Opposed to this model are continuous models of the water structure.[11-12] The proponents of continuum theories emphasize the continuous evolution of the broad bands, rather than trying to deconvolve them into substructures. From our point of view, the discrepancy between these two classes of the theoretical models appears to be more semantic, and they are supplementary rather than contradictory. In recent study of infrared spectra of aqueous dispersions Hübner et al.[13] have pointed out the danger of interpreting complex spectral bands solely on the basis of spectral shifts. They cite examples where deconvolution of the complex band explains the spectral shift in terms of discrete components, while the frequency shift of overall line contour leads to the opposite conclusions about the phase transition studied. The main argument against the structural (mixture) models of water is based on a statement that those models are not able to explain the entire collection of empirical data from spectroscopy, thermodynamic,

and neutron diffraction. Nevertheless, in some recent papers[14-15], spectroscopic studies of the $2v_1 + v_3$ combination band (960 nm) in a wide range of pressures and temperatures has led to a reconsideration of the mixture model involving three species. In these papers, certain features of the continuum model are retained by use of the concept of energy bands[10] rather than discrete sharp energy levels. This model proposes a distribution of the hydrogen bond energies grouped around three component bands S_3,S_1 and S_2, i.e. a model featuring a relatively small number of distinguishable molecular species with continuous distribution of hydrogen bond length and angles associated with each specie. The combination band peak has been resolved into three gaussians with constant positions and widths.[14-15] Similar results have been presented by V.Fornes and J.Chaussidon[16] for the $v_2 + v_3$ first combination tone of water molecules. Both groups elaborate quantitative results for the energy of the hydrogen bond formation (rupture). All of the above mentioned investigators derived their data by fitting the spectral bands to the sum of two or more gaussians, in most cases with the aid of an analog "curve resolver".

Recent advances in multivariate statistics and low-noise NIR spectrometers provides an impetus for restudy of the spectra of pure water as a function of temperature. Coupled with advances in instrumentation for high precision data acquisition are advances in data analysis. At present, there seems to be no existing methodology for quantitatively deciding the number of species contributing to water spectra. Clearly, arguments based upon the existence or absence of isosbestic point do not appear definitive nor do observations of spectral shifts of the mean position of complex peaks. It is the purpose of this paper to describe a technique for obtaining a lower bound to the number of species contributing to a series of spectra taken as a function of some external variable(e.g. temperature, pressure) within the linear additivity constraint. This technique which we call "Chemical Regression" was first proposed by Box and later described fully by Lawton and Sylvestre[17,18] The method to be described more fully in the theory section relies on a description of the spectra in form of linear combination of the eigenvectors of the spectral data matrix. Criteria are available to determine a lower limit to the number of eigenspectra required to describe the signal variance while eliminating the noise

variance. If the number of eigenspectra is small it can be argued that the mixture model has merit. On the other hand, a finding that a large number of basis vectors must be retained might be used to bolster the continuum model. Not only can a lower bound to the number of components be found, but also estimates of the spectra associated with each species can be obtained. This is accomplished by rotation of the abstract eigenvectors into a set of vectors which obey physical constrains appropriate to the problem. Thus the necessity to assume that the spectral shapes of the components is gaussian is eliminated and the spectral profiles are derived directly from the data. Constraints may be imposed not only on the spectra(e.g. positivity) but may also be imposed upon the way in which the intensity varies with the external variable (i.e. we may postulate a model for the effect of physical variance and derive the physical parameters by least square fitting). Thus it would appear that chemical regression potentially provides further insight into the mechanism for spectral changes of water with temperature, yielding estimates for the number of species involved, the thermodynamic parameters governing their interrelationship and estimates of the spectra of each.

In this study we have used this new method to reexamine the 960 nm combination band in pure water. This band demonstrates a strong dependence on temperature changes and has a well defined isosbestic point, that could be a sign of the presence of two or more species in pure water. Another important reason for choosing the SW-NIR range for examining the structural model of water is connected to the evident fact that in this range the shift between the spectral components-species, if they do exist, would be more distinguishable[3], and their separation could be less ambiguous.

Experimental. The measurements were made with an in-house constructed SW-NIR diode-array spectrometer[19] and a 4-cm optical pathlength quartz cell, and repeated with the Hewlett Packard diode array spectrometer HP-6582A and a 2-cm cell inside the HP-spectrometer. In the case of the home-made spectrometer, the radiation was delivered to the cell with a fiber optic, which made temperature control more convenient and reduced fog on the windows. Temperature control was achieved by equilibrating the sample cell in a water bath at a fixed temperature. The temperature of the cell was measured with a thermocouple and the signal was digitized and registered on the

computer's hard disk simultaneously with the digitized spectroscopic data from NIR spectrometer. The measured temperatures are believed to be correct to within 0.5°C. The spectra of the pure distilled and deionized water in the spectral range 850-1100 nm were taken over the temperature range 10 - 80 °C. The cell filled with CCl_4 was used as reference. The spectra are depicted in Figure 1. The spectra contain visible baseline offset and a slope. The nature of this bias and it's subtraction are discussed below. Nevertheless, we did not take special measures to improve the absolute measurements of the temperature, but the rate of the spectral scanning (60 scans per second) allowed us to reduce the noise by repetitive averaging. We believe that our experimental data for the studied combination band are the most precise at this time.

Results and Discussion. The temperature dependent offset could be referred to the changes of refractive index of water with the temperature. Fresnel reflection R changes according to the expression:

$$R = (n-1)^2/(n+1)^2 , \qquad (1)$$

where $n = n_q/n_w$, n_q and n_w are refractive indexes of quartz and water respectively. The changes in n_w in the entire temperature range are less than 1.5% and corresponding change in R are of order of 0.01. Taking into account that the cell has two interfaces with water and the effective absorbance will increase with the temperature (the refractive index and the reflectance are respectively decreasing), the baseline shift is estimated to be within 0.02 absorbance units, in good agreement with observed data. Now, understanding the nature of the baseline offset we can subtract it. The bias that is due to the strong absorption bands existing in the vicinity of the investigated peak could be approximated by the straight line and subtracted in the same way. After subtracting the offset and the slope the spectra appear more regular (Figure 2). We have taken into account the changes of the water density with the temperature. These small corrections are within 1.5% of the absorbance value.

In order to build a realistic model of water we need to determine the number of latent

variables that can describe the variance in the obtained spectra. There are different approaches to this problem. Most of them are based on the mathematical procedure of separating the noise or the bias from the real variance. This mathematical procedure is called Singular Value Decomposition (SVD). It consists of representation of the spectral matrix of absorption **A** in the form:

$$\mathbf{A} = \mathbf{USV'}, \tag{2}$$

where **S** is diagonal matrix with the nonnegative diagonal elements in decreasing order, and **U** and **V** are unitary matrices, **V'** denotes the transposed **V** matrix. The columns of **A** represents the spectral vectors at a fixed temperature. The rows of **A** contain information about the variation in absorption at a fixed wavelength. We can also represent the experimental matrix **A** in the form

$$\mathbf{A} = \mathbf{DC} + \mathbf{E}, \tag{3}$$

where matrix **D** contains only spectral components of the mixture and, the matrix **C** represents the concentration of the different components depending on the variable parameter (in our case the temperature). Matrix **E** contains experimental noise. From Eqs.(2) and (3) we can derive an equation:

$$\mathbf{DC} = \mathbf{USV'}, \tag{4}$$

where

the bars denote truncated matrices containing only the vectors and eigenvalues which are meaningful for the problem, namely they take into account the variance in the spectral matrix **A** and reject the noise. The representation of the experimental matrix **A** in the form of Eqs.(3) and (4) is well known as Principal Component Analysis (PCA).[20] PCA is a powerful tool in separating the noise from the real spectral components and estimating the most likely number of latent variables (meaningful singular eigenvalues) in the matrix **A**, that can describe the variance in **A** with reasonable precision. Since the determination of the number of "real" Principal Components and elimination of those which describe the

variance of the noise is an ambiguous task, we use auxiliary techniques, such as Evolving Factor Analysis[21]. The main concept of EFA is a graphical representation in which normalized (divided by the trace) singular values of the submatrices of matrix **S** in descending order versus the constituent, are displayed and examined for emerging eigenvalues. EFA has been used to analyze spectra consisting of strongly overlapped peaks[22]. The normalized eigenvalues usually are depicted on a logarithmic scale. For the matrix **A**, corresponding to the spectra shown in Figure 2, EFA evidently shows three emerging eigenvalues. The results of EFA are illustrated in Figure 3. The investigation of the next spectral eigenvectors from matrix **U** shows that they contain much more noise than the first three, and hence they are useless for constructing the set of real spectral components. Therefore, PCA analysis suggests the same rank of three. Consistent with the estimation of rank three is the structure of the spectral eigenvectors as shown in Figure 4. These eigenvectors are largely free of noise. Examination of the higher eigenvectors showed them to be highly contaminated with noise (Figure 5) and too irreproducible to be of value in representation of our data set. Hence within our current signal level and reproducibility, a basis set of three components seems defensible.

Now, starting with the assumption of three components, we can try to rotate our spectral eigenvectors (Figure 4) to the set of real spectral peaks. The procedure of nonlinear regression based on the postulated reaction has been described by Shrager[22,23]. This procedure of recovering the real spectral components and concentrations (titration), namely calculating the matrices **D** and **C** from the matrices **U**,**S** and **V** implies that one makes some reasonable assumptions about the kinetics of the system under consideration, and then finds the transformation which fits the rotated vectors of the **V**-matrix (so called "scores") to the imposed model. After making the decision about the rank of the data, the next step is to postulate a model for the kinetics of the reaction. This will, in turn, provide the means for recovery of the pure spectral components and the equilibrium constants. From the above described analysis of the rank of our spectroscopic data, it follows that there are three distinguishable molecular species in pure water. The postulation of thermodynamic equilibrium among all three

species leads to a set of equations for the concentrations $\mathbf{C}_j$ of different species :

$$\begin{aligned} C_2 &= C_1 \exp(-\Delta H_{12}/RT + \Delta S_2), \\ C_3 &= C_1 \exp(-\Delta H_{13}/RT + \Delta S_3), \\ C_1 &+ C_2 + C_3 = 1 , \end{aligned} \qquad (5)$$

where the $\Delta \mathbf{H}_{ij}$ and $\Delta \mathbf{S}_j$ are the relevant enthalpies and entropies of the imposed reaction. The equilibrium constants are: $K_1 = C_2/C_1$, $K_2 = C_1/C_3$, $K_3 = C_2/C_3 = K_1K_2$, and $\log(\mathbf{K})$ versus reciprocal temperatures $1/T$ are linear functions. Under these assumptions we can rotate the titration eigenvectors from **V** with the aid of 3 by 3 matrix **T**, in order to yield the equation:

$$\mathbf{V' = TC.} \qquad (6)$$

Comparing Eqs.(2) and (4) we can derive the matrix **D**, containing the pure spectral components,

$$\mathbf{D = UST.} \qquad (7)$$

The problem of calculating the transformation matrix **T** is central to this nonlinear regression procedure. We used the Nelder-Mead simplex optimization algorithm, that solved Eq.6 with four unknown nonlinear parameters ΔH_{12}, ΔH_{13}, ΔS_2 and ΔS_3, and nine unknown linear parameters, that actually determine the matrix **T**, in the least square sense. The routine returns the unknown parameters and the norm of the difference vector between the functions C_j from Eq.5 and rotated vectors **V**, that serves as a measure for this nonlinear fitting. The original "scores" from the **V** matrix and rotated to the real concentration C_j are depicted in Figures 6 and 7 respectively. Now after calculating the **T** matrix we can recover the pure spectral components with the aid of

Eq.7. Three spectral components shown in the Figure 8 were recovered with the above described nonlinear regression technique. Figure 9 shows the spectral components recovered from different data, obtained from different spectrometers, and demonstrates the level of confidence in recovering the spectral components with the chemical regression. The returned enthalpies for the reactions ΔH_{ij} are: $\Delta H_{12}=2.6$ kcal/mol, $\Delta H_{31}=3.6$ kcal/mol. The first one corresponds to the well known value of the heat of hydrogen bond formation in pure water. The latter is probably the heat of formation of the intermediate form of hydrogen bonded specie in water. This dependence is very sensitive to the recovered nonlinear parameters and should viewed qualitatively rather than reflecting real entropies and enthalpies of the hydrogen bond formation. Stability analysis of this nonlinear regression procedure have been made, by adding artificial random noise to the experimental spectral data. The routine of chemical regression demonstrates high stability in recovering spectral components but fairly poor reproducibility for concentrations. This feature of chemical regression is not unknown but has to be understand in terms of illposed problems[18]. The values cited above correspond to the spectral components depicted in Figure 8 and are probably not very reliable, but the shape of the recovered spectral components are reproducible for different sets of data and demonstrates high stability upon small random perturbation of the initial spectral data. Using pseudoinverse operator and recovered spectral components we were able to calculate the experimental concentration matrix $\mathbf{C}_{exp}$ (closed circles in Figure 7) from the matrix **D**.

$$\mathbf{C_{exp}} = \mathbf{pinv(D)A} \qquad (8)$$

pinv in Eq.8 denotes operation of pseudoinversion, according to definition **pinv(A)A** = **I**, were **I** is a unity matrix.

The spectrum which belongs to the specie which dominates at high temperature is the most blue shifted and narrowest of the spectral components, indicating the least amount of hydrogen bonding. The spectrum from the specie which exist through the range of

temperatures is intermediate in spectral shift and width. The low temperature specie is the most red shifted and broadest consistent with a high degree of hydrogen bonding, and reflects the statistical nature of the different length of hydrogen bonds in water clusters. Thus the evolution of the spectra is in agreement with the many studies of effect of hydrogen bonding on spectra.

Our analysis of the temperature dependent spectra of the 960 nm combination tone peak demonstrates that the three spectrally and structurally distinguishable species are needed to explain the evolution of the spectra within the framework of a simple thermodynamic model. The attempt to deconvolve the spectra imposing a two species model (bonded and nonbonded structures, being in thermodynamic equilibrium) derives unrealistic spectra of the components and thermodynamic parameters. It seems very probable that more precise spectral data and absolute temperature measurements would lead us to reconsideration of the minimal number of species needed and consequently the imposed thermodynamic model. Such studies would demand a substantial improvement of the spectroscopic apparatus and probably a more diverse approach to this problem, exploiting different methods of CARS spectroscopy of Raman-active vibrational transitions or more precise investigation of lower overtones in the NIR range of water spectra. Such studies are complicated by the high level of noise due to the high extinction coefficient and problems of temperature and flow control inside very thin cells.

Conclusions. In this study we, for the first time, applied the powerful technique of multivariate statistics and nonlinear regression to the problem of water structure. Our findings support the mixture model of water with at least three species. For the first time, we recovered the pure spectra of these species from an imposed explicit physical model. Nevertheless, at this time we don't have a clear understanding of the physical nature of these species and the relevant energies of reactions. However, this model can be used as an analytical approach to the interpretation of water spectra and even for measuring the temperature of the water-containing samples. The obtained spectral components can be exploited for developing a statistical theory of hydrogen bonding in water and can be helpful in verification of the numerous theories[24,25] which try to calculate the shape of the

absorption and Raman band in pure water. The pure components found from the temperature dependent spectra of pure water could be used for interpretation of the temperature dependence of the NIR spectra of human tissue and for improving of the quantitative prediction of the depth of burn wounds.

II. Fundamental Studies of Dynamic Properties of Human Skin.

A. Temperature Studies of Skin of Live Human Subjects.

Introduction. When skin is burned, even slightly, the body responds by increasing blood flow to the injured area. This is accomplished by dilating the capillaries nearby. A similar response is observed when heat is applied locally without burning. Increases in body temperature, through increased metabolism and increased ambient temperature induce vasodilation on a larger scale as a heat exchange mechanism. Reflectance spectroscopy should detect primarily an increase in hemoglobin and water and, as a side benefit, measure the local temperature.

Experimental. Spectra were taken from the forearms of seven people at temperatures ranging from 9 to 35°C. The subjects had skin types varying from very fair to oriental. Four were female and three were male. The skin was cooled with water and ice and heated with a heat lamp, allowing five to twenty minutes for stabilization. Temperature was measured with a small thermistor at the surface of the skin. The data were analyzed by step-wise linear regression[26] and various forms of principal component regression, using several preprocessing methods.

Results and Discussion. One subject was studied in detail from 9 to 36°C. Figure 10 shows second derivative spectra for the range 900-1400 nm. The largest variations appear at 1150 and 1213 nm. Difference spectra were computed using the spectrum taken at 9°C as a reference (Figure 11). The large peaks at 969, 1154, and 1388 nm in the difference spectra are attributed to the sharpening of the water peaks at elevated temperatures (Figure 12) and not to an increase in water concentration. The 1213 nm absorbances are attributed to fat.

Similar results were observed in all seven subjects. Again, the second derivatives were calculated and the spectra representing the coldest temperatures were subtracted.

Although each subject was tested at a different range of temperatures, the same relative changes appear each time. Spectral changes from 1350 to 1800 nm are irregular and may be influenced by skin oils or sweating (or perhaps just instrumental noise, as these spectra were acquired before the instrument was optimized). The subjects were divided into two groups. The first group contained 3 subjects (18 spectra), the second contained the remaining 4 subjects (20 spectra). Step-wise linear regression was used to build three wavelength models using data from these two groups. Both models used similar wavelength sets (1016,1073,1156 and 1001,1076,1150) The 1150,1156 and 1001,1016 nm wavelengths correspond to the spectral change of pure water. Each model was used to predict temperatures of the subjects in the other group (Figure 13). The standard errors of prediction (SEP) were 1.3° and 1.4°, approximately equal to the estimated accuracy of the reference method (1.5°C). The correlation coefficients were both 0.982.

Biologically, it makes little sense to suggest that fat (1215 nm) disappeared during temperature induced vasodilation while the water concentration neither increased nor decreased significantly. The apparent changes are much too large and rapid to be caused by metabolism. It is more probable that these spectral changes are due to a change in the structure of the skin during vasodilation and corresponding changes in effective path lengths of light through the dermis and the fatty layer below. These results suggest that it may be possible to follow, quantitatively, inflammation of burn wounds both in response to the injury and to infection.

B. Ischemia.

Introduction. Ischemia, insufficient blood flow, occurs wherever circulation is restricted by mechanical means or by damage to blood vessels. The blood stagnates and deoxygenates as the surrounding tissues continue to consume available oxygen. Eventually the tissues themselves become deoxygenated and dysfunctional. Ischemia can be a significant factor in prognosis of partial thickness burns. A burn may initially appear to be shallow, but if the circulation has been compromised, skin becomes

ischemic and dies, producing a full-thickness burn in a few days.[27] Pulse oximeters can measure the oxygenation of blood spectroscopically[28,29] but they use probes that must touch the skin, and they require a strong blood flow at the site tested. Therefore, they are not applicable to either burn wounds or ischemia in general. With our non-contacting reflectance probe, however, it seemed possible to determine the oxygenation of blood in a burn and to deduce whether it is sufficient to allow the wound to heal. Accordingly, the following experiments were conducted to test this hypothesis.

Experimental. Ischemia was induced in the forearm of a healthy volunteer by applying a pressure cuff (150 mmHg) for 8 minutes. Spectra were recorded in the visible region (450-780 nm) every 20 seconds. The pressure was then released and circulation returned to normal. The second derivative spectra were analyzed to reveal the number of independent spectral components and their patterns of variation. Principle component analysis (PCA), a multivariate statistical method which does not require independent measurement of constituent concentrations, was used for analysis.[19]

Results and discussion. Figure 14 shows spectral shifts that occur during ischemia. The two bands of oxyhemoglobin are clearly visible. Over time they are replaced by the broad deoxyhemoglobin band at 555 nm. The smaller 760 nm band of deoxyhemoglobin is also visible. PCA resolves the spectra into two components (Figures 15a, 15c) corresponding to oxy- and deoxy-hemoglobin respectively. The behavior of these components agrees with the known physiology of ischemia; when the circulation is restricted, the blood becomes deoxygenated. When the restriction is released, the initial surge of new blood causes a hyperemic increase in blood volume which gradually returns to normal equilibrium.[30] Figures 15b and 15d show scores calculated by PCA, the estimated concentrations of oxy- and deoxy-hemoglobin that were derived from the spectra. The deoxygenation (0-8 min.), overshoot (8 min.), and reestablishment of equilibrium (8-16 min.) are clearly visible.

C. Healing in a Shallow Burn.

Introduction. Shallow burns, although of little interest to a burn surgeon, provide us with a relatively simple model of inflammation and healing in minor injuries. Inflammation increases circulation, bringing extra blood to the injury. In areas where the circulatory system has been damaged, blood flow may be restricted and the hemoglobin may become deoxygenated. Both of these phenomena have been observed with a visible/near-infrared spectrometer. When one of the students here burnt himself, we had an excellent opportunity to refine our technique and to verify that our instrument would indeed detect the expected circulatory changes in an injury. We were also able to study the burn almost daily for two weeks, something which has proved difficult with hospitalized patients.

Experimental. The burn studied was on the upper arm of a white male, age 24. It was caused by contact with a hot stove pipe. The burn appeared dark brownish red and developed two small blisters. Four areas were chosen for study: an area of apparently normal skin 2 cm from the burn, a light brown area at the edge of the burn, and at each of the two blisters. The burn was studied 1-5, 9-11, 15-17, and 29 days after the injury. Reflectance spectra in the region 450-780 and 900-1800 nm were obtained with the modified LT spectrophotometer, using both silicon and lead sulfide detectors. The burn and detector were covered with a black cloth to exclude room light during measurements. All data were taken at room temperature, which fluctuated over a range of 15 C°. Second derivatives were calculated and then analyzed by PCA.

Results and Discussion. The visible and NIR spectra of the burn on the first day are presented in Figures 16 and 18. Spectra of the three burned and one unburned areas are reasonably similar as the damage was not extensive. The main differences are the large increases in oxyhemoglobin bands and the decrease of the 760 nm deoxyhemoglobin band in the spectra of the burned sites, due to capillary dilation. Changes in the NIR spectra are consistent with those observed in the vasodilation

experiments. Also apparent is the large variability in the average optical density from sample to sample. This effect is ascribed to reflectance at the skin surface and the irreproducibility of sample positioning. These factors were largely irrelevant in this experiment, and were removed by derivative calculation (Figures 17, 19). They will, however, be important for the modification of the Burn Depth Imager built previously[31] which does not have the ability to calculate derivatives.

Analysis of all of the spectra (four sites over 29 days) with PCA suggests that there are three components in the visible region and one in the NIR which differ between the burned and unburned sites (Figures 20, 21, 22, 27). The scores (estimates of concentrations) of these components show a rapid change during the first three days followed by a slow return to normal (Figures 23, 24, 25, 29). The first two components in the visible region (Figures 26, 27) are quite similar to the first two components of the PCA of ischemia which correspond to oxy- and deoxy-hemoglobin. The large peak in the third component (Figure 22) has not yet been identified though it has appeared in other experiments. It may be a distorted methemoglobin peak or another metaloprotein (carboxyhemoglobin, cytochrome oxidase,...). The two components of the NIR spectra represent surface reflectance (Figure 26, 28) and vasodilation (Figure 27, 29) respectively.

The spectra taken from the shallow burn as it was healing manifest gradual increase in the absorbance at 1213 nm (Figure 30, 31). This is caused by the decrease of inflammation and vasodilation over time. However, all of the spectra taken on the 5th, 9th, and 29th days, including those from unburned skin, have absorbances at 1215 which are less than would be expected. It was known that the room temperature varied considerably during the study and this may have affected the data. Since no temperature data had been collected during the study, the three wavelength model for skin temperature was applied to the spectra of the burn. It was shown that the irregular results obtained on days 5 and 29 could be attributed to unusually high temperatures on those days, and the skin temperature model permitted some temperature correction in the burn spectra. But the model, based on localized temperature induced inflammation, did not fully explain variations caused by whole body heat exchange mechanisms. More

work needs to be done before temperature correction can be done on burn spectra, but it may prove easier to correct the spectra mathematically than to control the temperature of the patient.

III. Studies of Burns in Human Subjects, Harborview Hospital.

Experimental. Reflectance spectra were acquired from 25 patients who were selected to give a representative sample of superficial, partial and full thickness burns. Children and elderly patients were excluded. Data was collected on the third day post burn, immediately after tanking. Both the LT spectrometer and the video Burn Depth Imager (BDI)[31] were used. The attending physicians were asked at that time to predict whether or not those burns would heal within 21 days.

Two case studies are included here to illustrate the types of results obtained by the LT spectrometer. The first case illustrates typical results for shallow and full thickness burns. The second case demonstrates the usefulness of the BDI and LT spectrometer for identifying deep burns, even when they appear shallow to the human eye.

A. Case Studies.

Case Study -- Patient #14. This patient had a small scald burn on her foot. Hot water had run down into her high-top boot, producing a shallow partial thickness burn at the top and a deep burn where the water pooled at the bottom. In spite of the depth of the injury, it was not grafted, because the patient was 8 months pregnant and the wound was not large. The patient was admitted on the third day after the injury because of infection and was discharged three weeks later, after the shallow half of the burn had healed. Spectra were taken on days 3, 4, 5, 7, 9, 10, and 11.

The spectrum of the shallow partial thickness burn (Figure 32) is similar to that of the superficial burn (Figures 16, 18). The main features are due to water and hemoglobin (Figure 33). The latter bands are quite pronounced because the removal of the epidermis exposed the capillaries. The triple lines mark the locations of the filters which were used in the BDI: the 560 nm filter measured a combination of oxy- and deoxy- hemoglobin, the 640 nm filter approximated a baseline, and the 880 nm band pass filter (880-1100 nm)

measured a combination of water and hemoglobin. [The sharp increase in the LT spectrum at 890 nm is caused by a filter change.]

The spectrum of the deep burn (Figure 32) was markedly different. The baseline was considerably higher and the water bands were less intense. The cause of these differences is uncertain at this time, but they are thought to be due to the physical properties (texture, light scattering, etc.) of the denatured dermis. The 560 nm hemoglobin bands are less intense, obscured by the layer of eschar. All of the above had been expected. The 640 nm filter, however, measured the shoulder of an unanticipated band at 630 nm. The intensity of the new band suggested that it was due to a derivative of hemoglobin, since few other biological compounds are as abundant and as highly colored. The band was attributed to acidic methemoglobin which has a band at 630 nm and is relatively common. Other derivatives may also be present in smaller quantities.

Case Study -- Patient #8. This patient had a flame burn on the dorsum of his hand. On the first day it appeared to be shallow, *and although* it developed a layer of eschar by the third day, it was still pinkish and was oozing blood. Based on its appearance, the attending physician predicted that it would not require grafting. The BDI, however, predicted that it had less than 30% chance of healing on its own. The spectrum (Figure 34) was similar to that of the shallow burn (Figure 32): low baseline and intense hemoglobin bands. The methemoglobin band, however, is clearly visible in the spectrum, though the resulting color change is not visible by eye. By the seventh day post burn, this had become a full thickness burn and it was then grafted.

B. Multivariate Analysis of the Aggregate Spectra.

Selected burn sites (n = 75) were followed by visual inspection for one month and classified according to outcome into two categories: Shallow (healed in less than 21 days) and Deep (grafted or healed in more than 21 days). Sites whose outcome was unknown (n = 9) were excluded from further analysis. The most common etiology was flame (52%), followed by scald (22%), chemical (8%), flash (8%), contact (6%), and grease

(4%). The mean age of the patients was 33 years and the mean TBSA was 6%. Subjects included 20 Caucasians, 3 Hispanics, and 2 Blacks.

The aggregate spectra (Figures 35, 36) in the visible region 450-760 nm (blue-green to red) were analyzed by PCA. Four major types of spectra variation (principal components, Figure 37) were observed. The first two have spectral features arising from the light scattering properties of dermis and eschar and the absorbance of venous blood. The third and fourth principal components correlated to healing time (Figure 38) and had spectral features similar to those of methemoglobin and oxyhemoglobin, respectively (Figure 39). A linear combination of these two (R, Table I) unambiguously differentiated between shallow and deep burns (Figure 40). [R = 10 * (eigenvector #3) + 2* (eigenvector #4), in arbitrary units.] The average values of R for shallow and deep burns were 5±4 and -7±7, respectively ($P < 0.001$). These predictions were significantly more accurate than the surgeons' (98% vs 88%, $n = 66$, $P < 0.02$, Table II).

C. Estimation of Methemoglobin.

The relative concentration of methemoglobin (M) was estimated by fitting each spectrum with a linear combination of the spectra of pure hemoglobins (oxy- and deoxy-hemoglobin and acidic and basic methemoglobin). These basis spectra are shown in Figure 41. Examples of the spectra which were constructed from the basis set and the corresponding burn spectra are shown in Figures 42 and 43. They do not fit exactly, indicating that the model is incomplete. Certainly the dermis and eschar have nonlinear effects on the spectra which have not been included, and there may be more than four species of hemoglobin as well. This simplistic model does, however, give an estimate of total methemoglobin. These results are listed in Table I and plotted in Figure 44. The resulting predictions are less accurate (85%) than those from the PCA model (R), indicating that the biochemistry and biophysics of these wounds is not yet sufficiently well understood, but they are similar enough to confirm that the BDI does indeed detect the elevated levels of methemoglobin in deep burns.

IV. Conclusions and Suggestions for Further Study.

With the LT spectrometer we are able to observe absorbance bands from most of the major constituents of skin. The instrument is sensitive enough to monitor changes as small as those induced by only a few degrees elevation in surface temperature. The techniques used are completely non-invasive, non-contacting, and non-destructive and require only a few minutes, making them suitable for use on burn patients.

The spectra acquired from hospitalized burn patients has given us new insight into the physiology of burn wounds. Severely elevated levels of methemoglobin have been observed in deep burns, even in burns which appear shallow for several days before becoming full thickness. Although the current Burn Depth Imager does inadvertently measure methemoglobin, it is not efficient and could be improved by a simple filter replacement (changing 640 nm to 630 nm). The spectrometers results, however, indicate that there are four major spectral components and it may be necessary to include a fourth filter for more accurate predictions. This will be explored further during the upcoming year.

Table I: Prediction Results

Site #	Depth	R	R pred.	M	M pred	Surgeons'
4-1-1	Superficial	0.6	shallow	62	deep	shallow
4-1-2		4.8	shallow	27	deep	shallow
16-1		7.0	shallow	4	shallow	shallow
16-2		4.0	shallow	6	shallow	shallow
20-1		7.9	shallow	34	deep	shallow
20-2		7.7	shallow	352	deep	shallow
28-1		2.0	shallow	13	shallow	shallow
28-2		5.2	shallow	10	shallow	shallow
1-1-1	Shallow	2.3	shallow	7	shallow	shallow
1-2-1		5.9	shallow	0	shallow	shallow
1-1-2		9.3	shallow	0	shallow	shallow
1-2-2		12.1	shallow	0	shallow	shallow
3-2		1.8	shallow	8	shallow	shallow
3-3		5.7	shallow	3	shallow	shallow
7-1		1.4	shallow	16	shallow	shallow
11-1		3.2	shallow	12	shallow	shallow
11-2		6.4	shallow	6	shallow	shallow
12-1		10.2	shallow	0	shallow	shallow
12-2		- 0.5	shallow	16	shallow	shallow
12-3		6.2	shallow	6	shallow	shallow
14-2		5.3	shallow	16	shallow	shallow
17-1		9.7	shallow	0	shallow	shallow
19-1-1		- 4.7	deep	20	deep	shallow
19-2-1		2.3	shallow	21	deep	shallow
19-1-2		5.5	shallow	10	shallow	shallow
19-2-2		4.1	shallow	14	shallow	shallow
21-1		4.7	shallow	12	shallow	shallow
21-2		10.0	shallow	0	shallow	shallow
21-3		10.5	shallow	1	shallow	shallow
22-1		4.1	shallow	10	shallow	shallow
22-2		7.2	shallow	9	shallow	shallow
22-3		1.8	shallow	14	shallow	shallow

23-3		- 0.6	shallow	23	shallow	shallow
23-5		0.4	shallow	22	shallow	shallow
27-1-1		11.8	shallow	0	shallow	shallow
27-1-2		13.1	shallow	0	shallow	shallow
27-2		10.2	shallow	0	shallow	shallow
29-1-1		2.6	shallow	8	shallow	shallow
29-2-1		7.6	shallow	0	deep	shallow
29-3-1		7.9	shallow	4	shallow	shallow
29-1-2		0.6	shallow	16	shallow	shallow
29-2-2		1.1	shallow	20	shallow	shallow
29-3-2		1.8	shallow	18	shallow	shallow
30-1		4.0	shallow	8	shallow	shallow
30-2		4.4	shallow	7	shallow	shallow
30-3		14.2	shallow	0	shallow	shallow
30-4		2.5	shallow	0	shallow	shallow
3-1	Deep	- 3.5	deep	24	deep	deep
6-1		-11.7	deep	32	deep	unknown
7-2-1		- 9.3	deep	34	deep	deep
7-2-2		-14.9	deep	20	deep	deep
8-1		-11.1	deep	27	deep	shallow
14-1		- 6.0	deep	26	deep	deep
19-3-1		- 2.5	deep	11	shallow	shallow
19-3-2		- 7.6	deep	21	deep	shallow
23-1		-28.1	deep	49	deep	deep
23-2		- 1.3	deep	39	deep	deep
23-4		- 1.2	deep	22	deep	shallow
24-2		- 0.8	deep	24	deep	deep
25-2		- 2.9	deep	18	shallow	deep
6-2	Full thickness	- 7.7	deep	20	deep	unknown
6-3		- 7.7	deep	21	deep	unknown
15-1		- 4.5	deep	33	deep	unknown
17-2		-15.3	deep	56	deep	deep
24-1		- 6.9	deep	29	deep	deep

Table II: Number of Correct Predictions

	# of samples	R	M	Surgeons
Shallow	47	46	40	47
Deep	19	19	17	10
% correct		98%	85%	88%

BIBLIOGRAPHY

(1) Afromowitz, M.A. "Spectroscopy of Burn Wounds"; annual report to the U.S. Army Medical Research & Development Command on Grant DAMD17-88-8125; University of Washington: Seattle, WA,

(2) *Water, A Comprehensive Treatise*, v.7; Franks F.; Ed.; Plenum: N.Y.,1981.

(3) *Structure of Water and Aqueous Solutions*; Luck Ed.; Verlag Chemie and Physik Verlag, Weinheim/Bergstr, 1974.

(4) Suhrmann, R.; Breyer, F. *Z. Physik. Chem.* **1933** *B20*, 17.

(5) Buijs, K.; Choppin, G. R. *J. Chem. Phys.* **1963**, *39,* 2035.

(6) Choppin, G. R.; Buijs, K. *J. Chem. Phys.* **1963**, *39,* 2042.

(7) Choppin, G. R.; Violante, M. R. *J. Chem. Phys.* **1971**, *56*, 590.

(8) Paquette, J.; Jolicoeur, C. *J. Solution. Chem.* **1977**, *6*, 403.

(9) Nemethy, G.; Sheraga, H. A. *J. Chem. Phys.* **1964**, *41*, 680.

(10) Senior, W. A.; Vand, V. *J. Chem. Phys.* **1965,** *43,* 1869.

(11) Eisenberg D.; Kauzmann, W. *The Structure and Properties of Water*; Oxford Univ.: N.Y. and Oxford, 1969.

(12) *Water and Aqueous Solutions: Structure, Thermodynamics, and Transport Process*; Horne, E.A., Ed. John Wiley & Sons: N.Y.,London, Sydney, Toronto, 1972.

(13) Hubner, W; Mantsch, H. H.; Casal, H. L. *Appl.Spectrosc.* **1990**, *44,* 732.

(14) Inoue, A.; Kojima, T.; Taniguchi, Y; Suzuki, K. *J. Solution Chem.* **1984**, *13*, 811.

(15) Inoue, A.; Kojima, T.; Taniguchi, Y; Suzuki, K. *J. Solution Chem.* **1987**, *16*, 727.

(16) Fornes, V.; Chaussidon, J. *J.Chem.Phys.* **1978**, *68*, 4667.

(17) Lawton, W. H.; Sylvestre, E. A. *Technometrics.* **1971**, *13*, 617.

(18) Sylvestre, E. A.;Lawton, W. H.; Maggio, M.S. *Technometrics.***1974**, *16*,353.

(20) Sharaf, M. A.; Illman, D.L.; Kowallski, B.R. *Chemometrics*; John Wiley & Sons; N.Y, 1986.

(21) Maeder, M. *Anal.Chem.* **1987,** *59*, 52.

(22) Shrager, R.I.; Hendler, R. W. *Annal.Chem.* **1982**, *54*, 1147.

(23) Shrager, R. I. *SIAM J.Alg.Disc. Meth.* **1984**, 5, 351.

(24) Coker, D. F.; Watts R. O. *J.Phys.Chem.* **1987**, *91*, 2513.

(25) Reimers, J. R.; Watts, R. O. *Chem.Phys.* **1984**, *85*, 83.

(26) Draper, N.R.; Smith, H. *Applied Regression Analysis*; John Wiley & Sons: New York, 1966; p 307.

(27) Panke, Thomas W.; McLeod, Charles G.,Jr. *Pathology of Thermal Injury: A Practical Approach*; Grune & Stratton: New York, 1985.

(28) Yoshiya, I.; Shimada, Y.; Tanaka, K. *Med. & Biol. Eng & Comput.* **1980**, *18*, 27-32.

(29) Mendelson, Y.; Ochs, B.D.*IEEE*, **1988**, *BME-35(10)*, 798-805.

(30) Hampson, N.B.; Piantodosi, C.A. *J. Appl. Physiol.* **1988**, *64(6)*, 2347.

(31) Afromowitz, M.A.; Callis, J.B.; Heimbach, D.M.; DeSoto, L.A.; Norton, M.K. *IEEE*, **1988**, *BME-35*, 842-850.

FIGURE CAPTIONS

Figure 1 Dependence of the experimental water spectrum on the temperature in the range 10-82$_o$C.

Figure 2 Water spectra after baseline subtraction.

Figure 3 Emerging eigenvalues from the Evolving Factor Analysis.

Figure 4 First three vectors of the U-matrix from SVD - loadings, 1-st vector - solid line, 2-nd - dashed line, 3-rd-dotted.

Figure 5 4-th and 5-th vectors of the U-matrix, contaminated with the noise.

Figure 6 First three vectors of the V-matrix, the notations of the lines are the same as in Figure 4.

Figure 7 Concentrations of the species vs reciprocal temperature, the notations of the lines are the same, as in Figure 4.

Figure 8 Recovered pure components of the water species.

Figure 9 Spectral components recovered from different data sets of spectra

Figure 10 Temperature variation in *in vivo* skin (2nd derivative)

Figure 11 Temperature variation in *in vivo* skin (2nd derivative, difference)

Figure 12 Temperature variation in pure water (2nd derivative, difference)

Figure 13 Prediction of temperature in *in vivo* skin

Figure 14 Ischemia (2nd derivative)

Figure 15 Ischemia: loadings and scores from PCA

Figure 16 Shallow burn (visible)

Figure 17 Shallow burn (visible, 2nd derivative)

Figure 18 Shallow burn (NIR)

Figure 19 Shallow burn (NIR, 2nd derivative)

Figure 20 Shallow burn (visible): 1st eigenvector from PCA, loading

Figure 21 Shallow burn (visible): 2nd eigenvector from PCA, loading

Figure 22 Shallow burn (visible): 3rd eigenvector from PCA, loading

Figure 23 Shallow burn (visible): 1st eigenvector from PCA, scores

Figure 24 Shallow burn (visible): 2nd eigenvector from PCA, scores

Figure 25 Shallow burn (visible): 3rd eigenvector from PCA, scores

Figure 26 Shallow burn (NIR): 1st eigenvector from PCA, loading

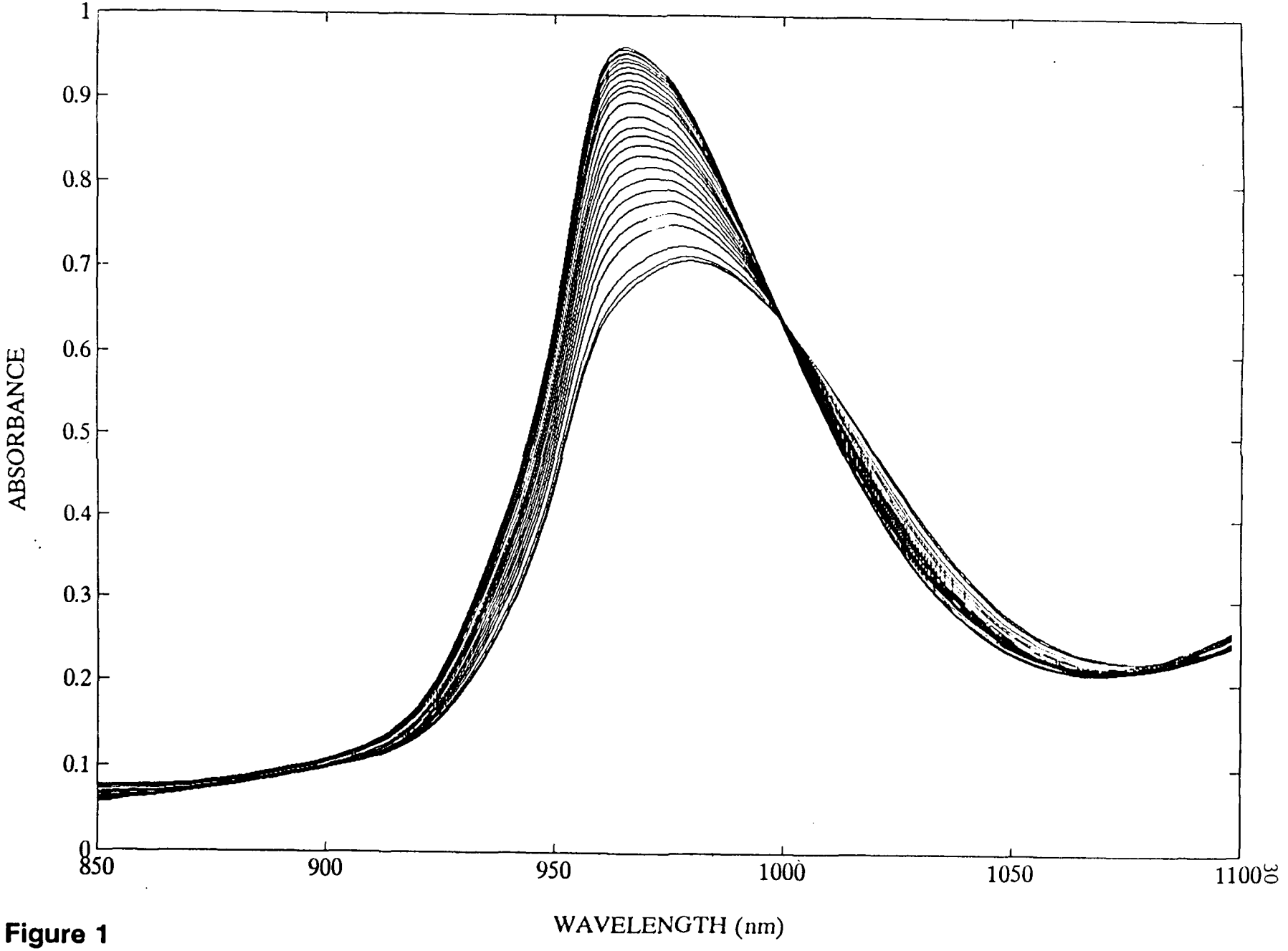
ABSORBANCE
WAVELENGTH (nm)
0
0.1
0.2
0.3
0.4
0.5
0.6
0.7
0.8
0.9
1
850
900
950
1000
1050
1100
30

Figure 1

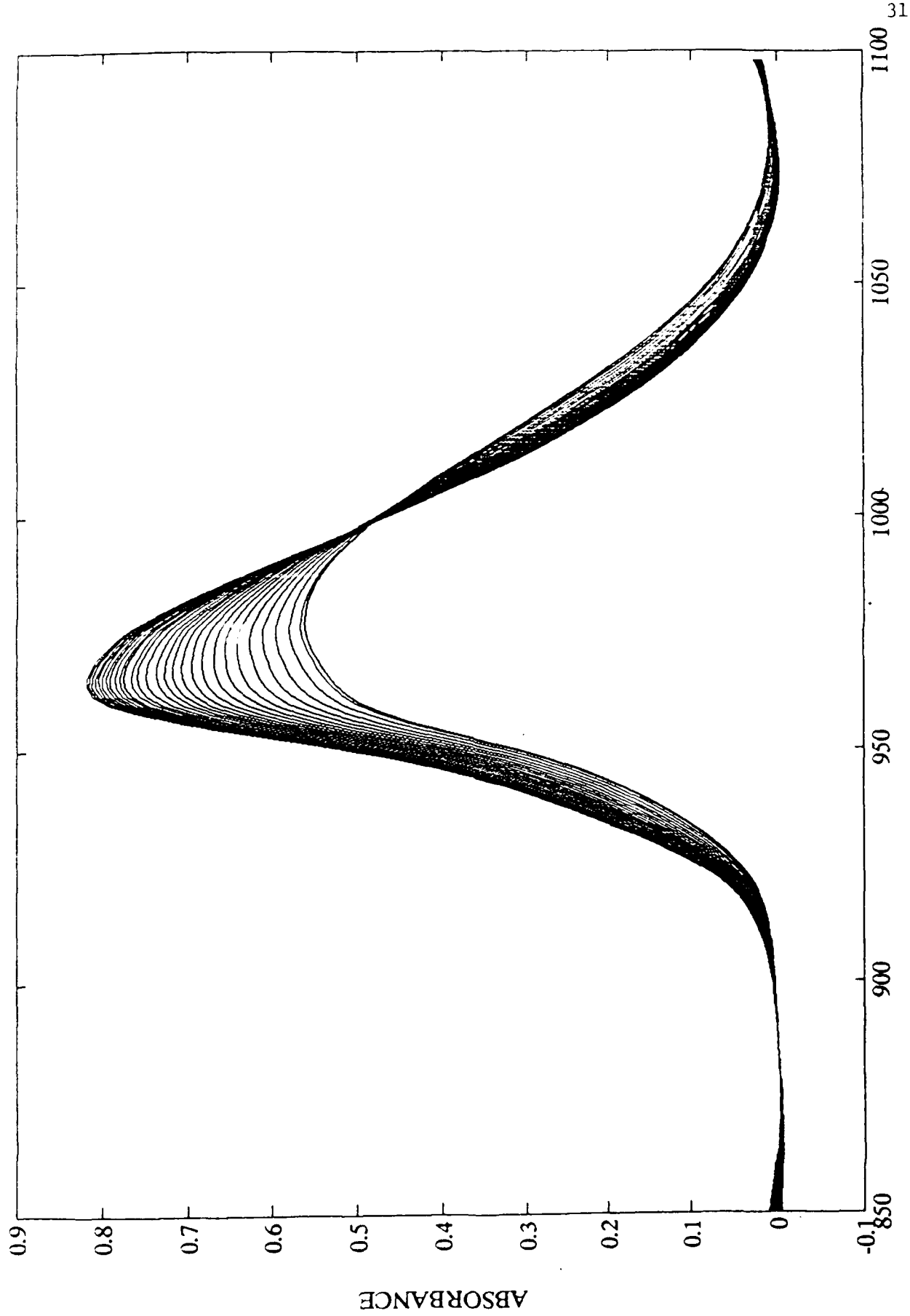
ABSORBANCE
0.9
0.8
0.7
0.6
0.5
0.4
0.3
0.2
0.1
0
-0.1
850
900
950
1000
1050
1100
WAVELENGTH (nm)

Figure 2

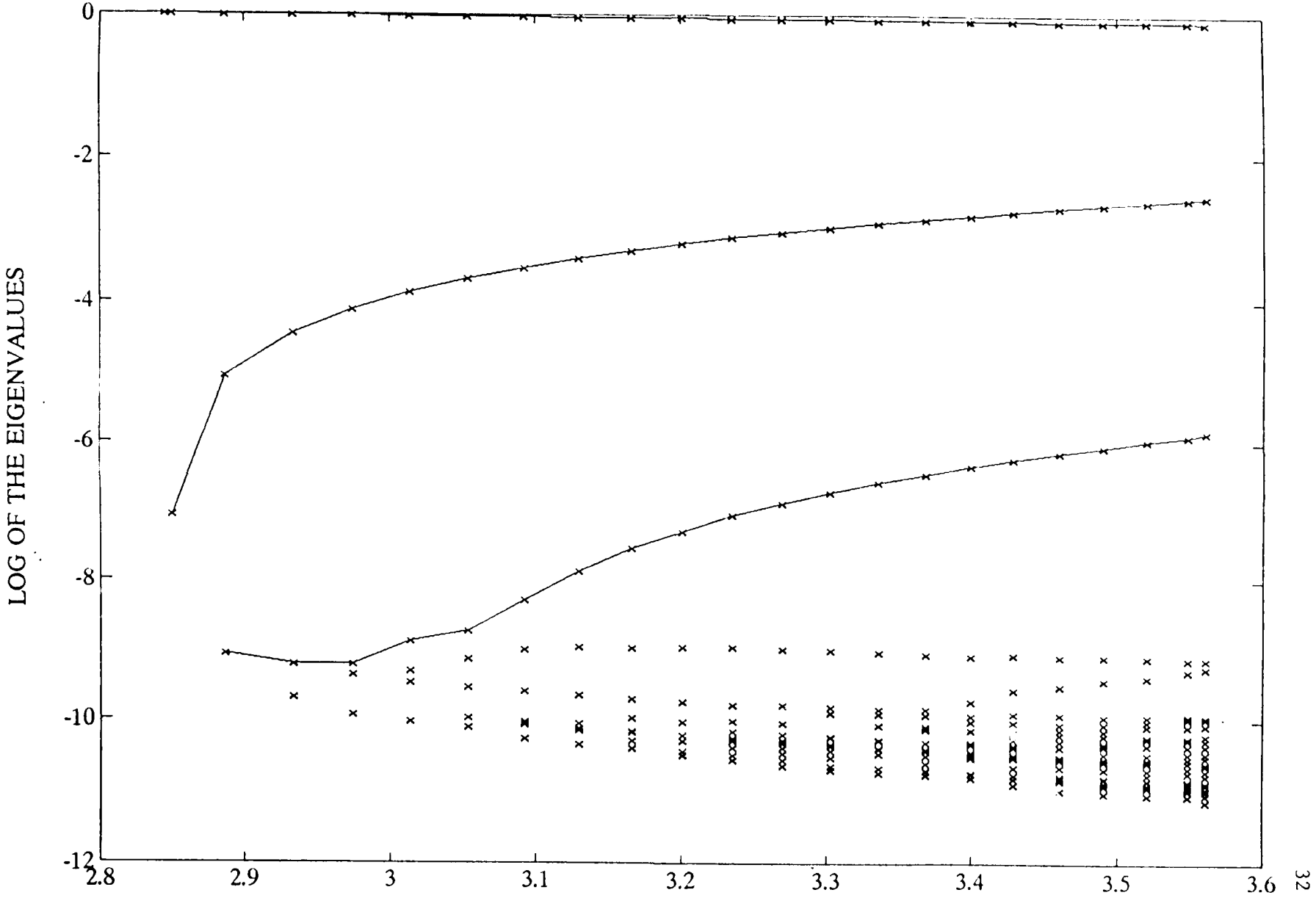
LOG OF THE EIGENVALUES
0
-2
-4
-6
-8
-10
-12
2.8
2.9
3
3.1
3.2
3.3
3.4
3.5
3.6
TEMPERATURE, 1/K
x10-3

Figure 3

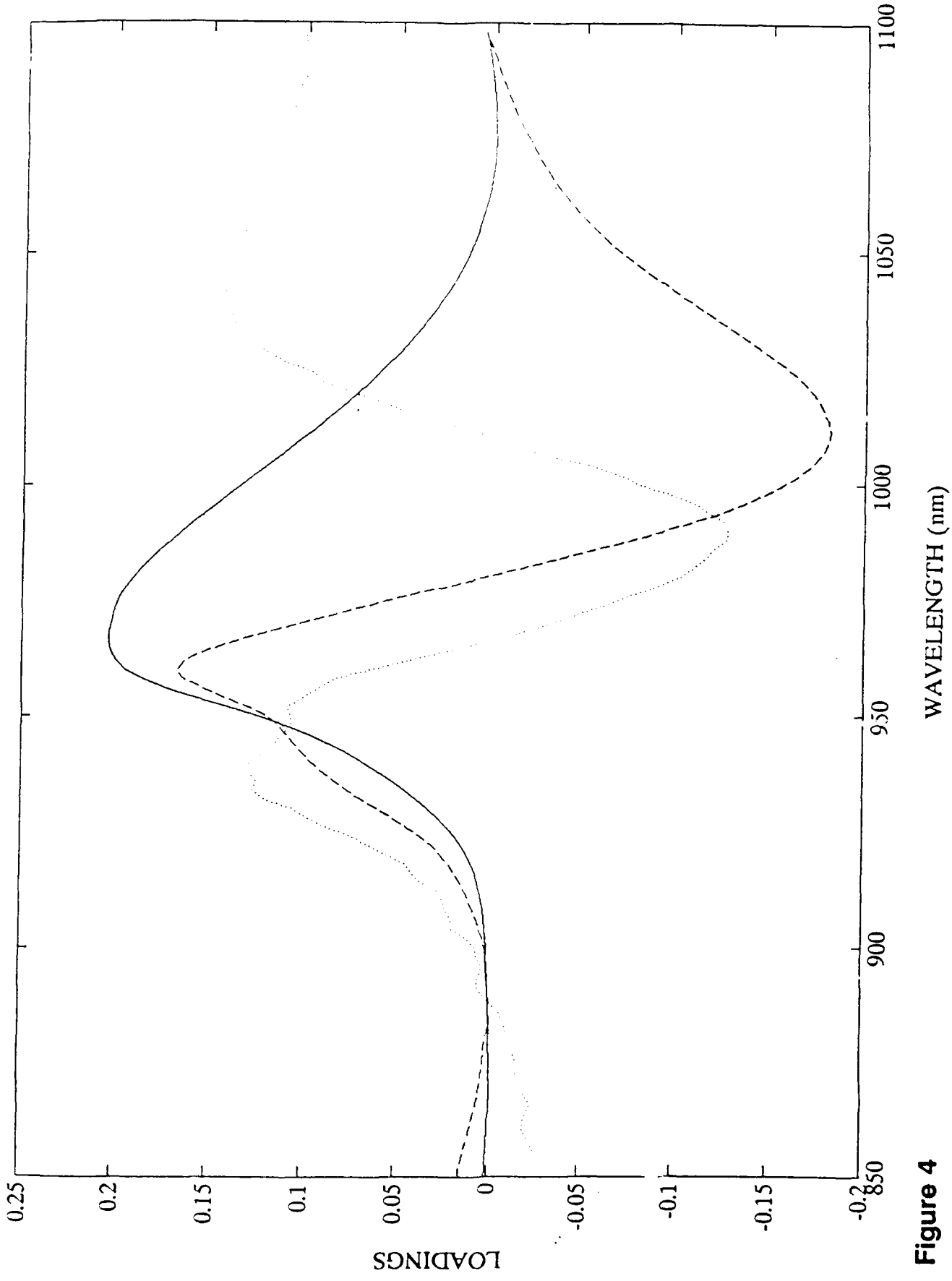
LOADINGS
0.25
0.2
0.15
0.1
0.05
0
-0.05
-0.1
-0.15
-0.2
850
900
950
1000
1050
1100
WAVELENGTH (nm)

Figure 4

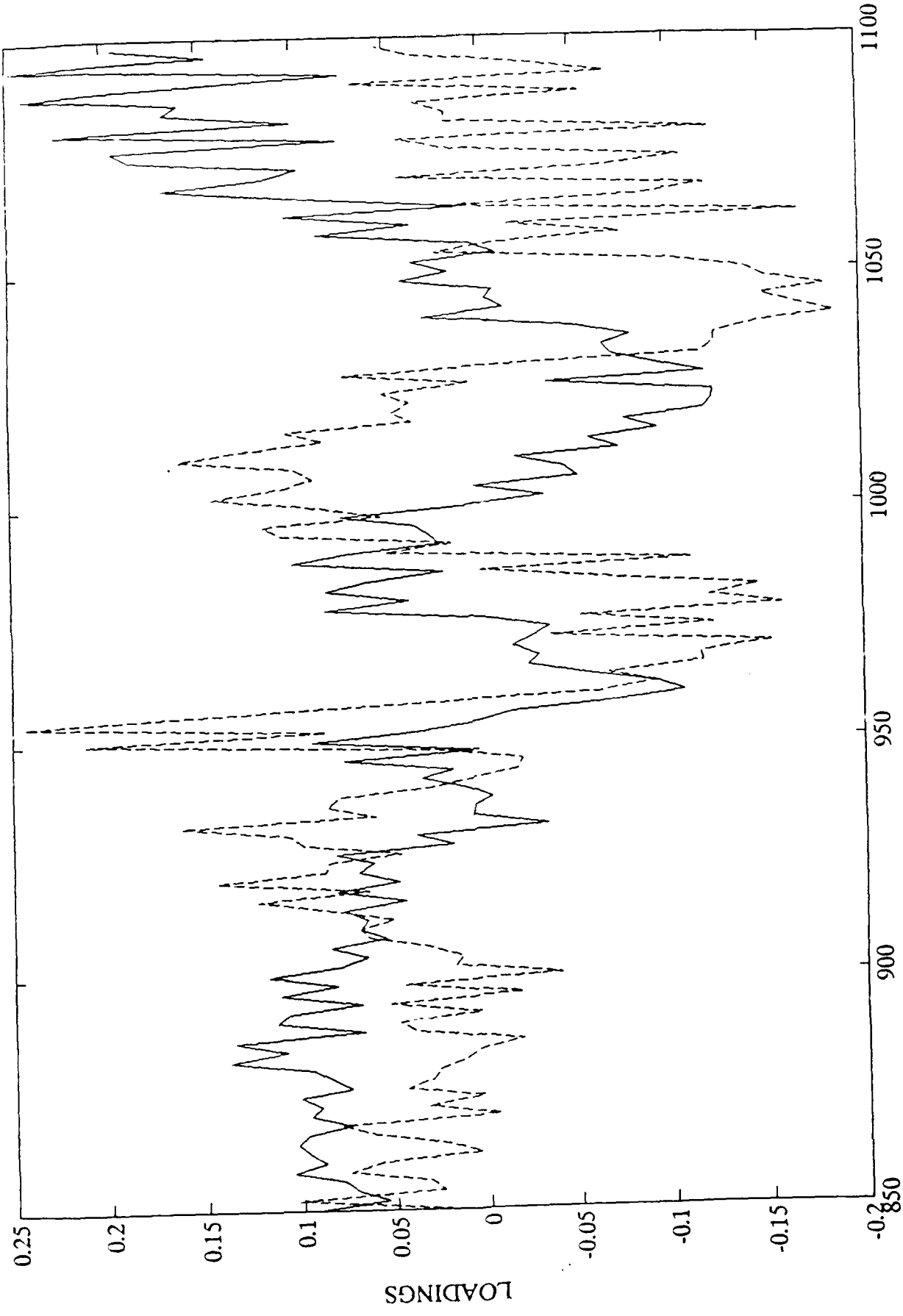
LOADINGS
0.25
0.2
0.15
0.1
0.05
0
-0.05
-0.1
-0.15
-0.2
850
900
950
1000
1050
1100
WAVELENGTH (nm)

Figure 5

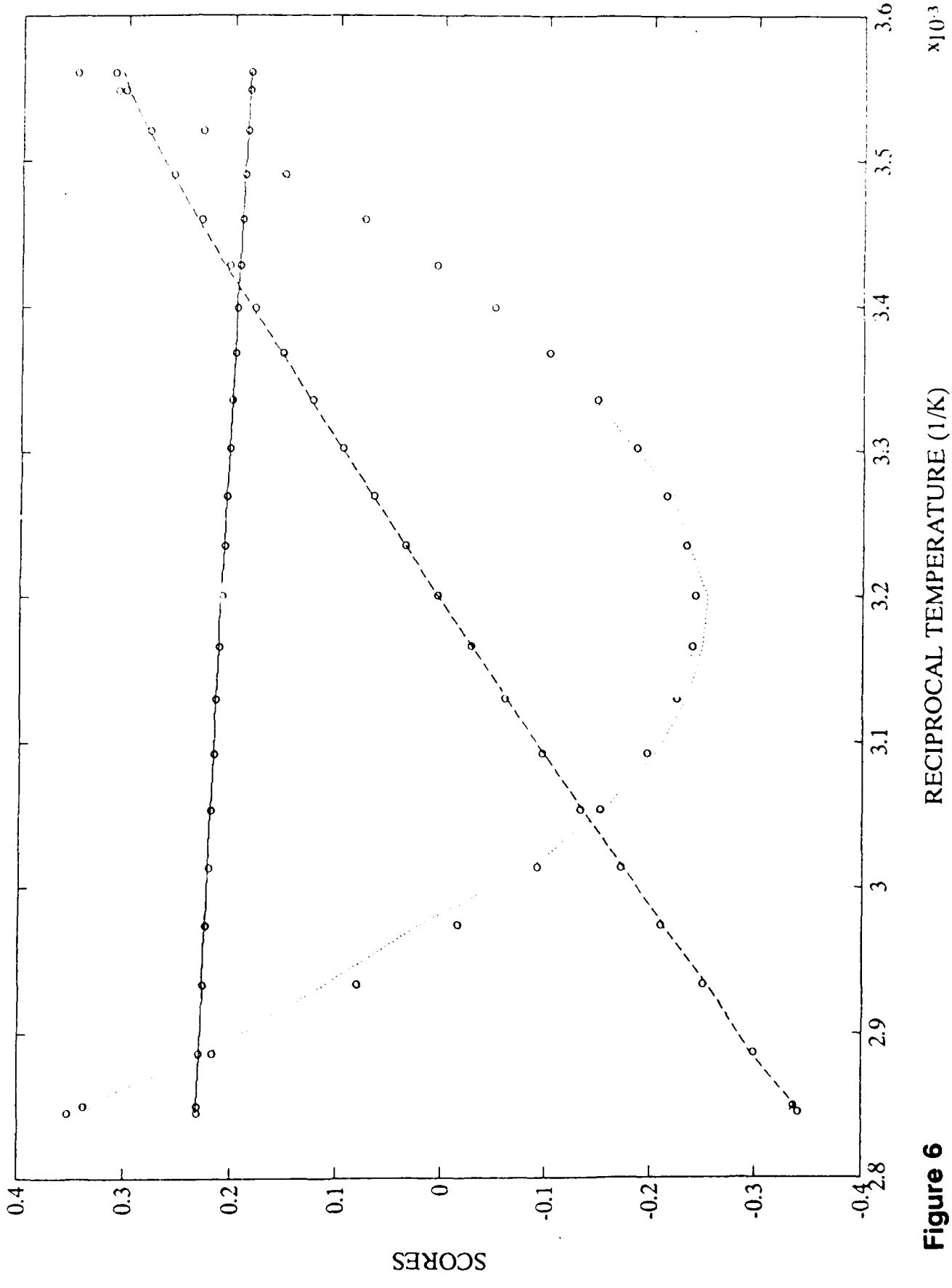
SCORES
0.4
0.3
0.2
0.1
0
-0.1
-0.2
-0.3
-0.4
2.8
2.9
3
3.1
3.2
3.3
3.4
3.5
3.6
x10-3
RECIPROCAL TEMPERATURE (1/K)

Figure 6

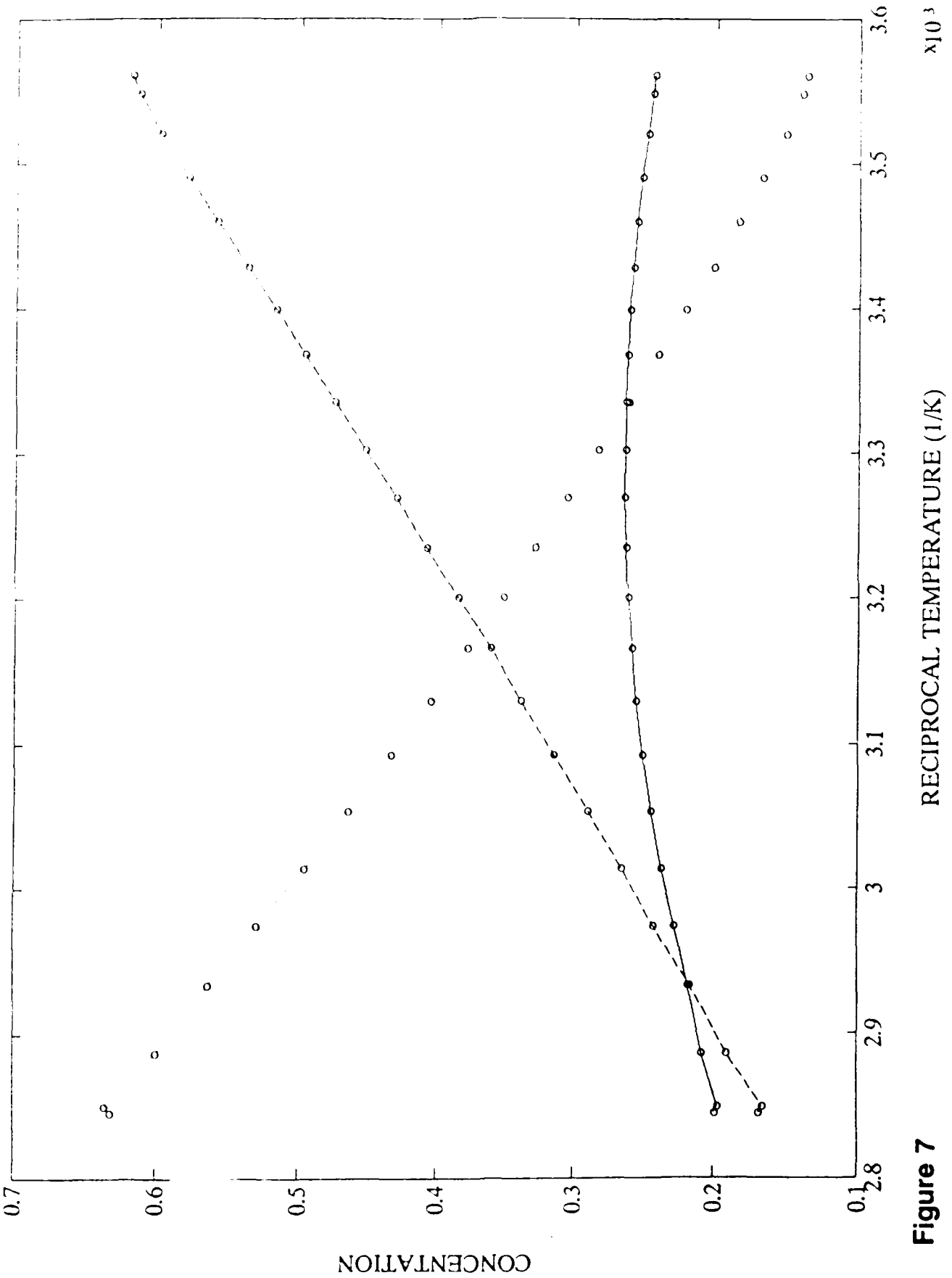
CONCENTATION
0.7
0.6
0.5
0.4
0.3
0.2
0.1
2.8
2.9
3
3.1
3.2
3.3
3.4
3.5
3.6
x10 3
RECIPROCAL TEMPERATURE (1/K)

Figure 7

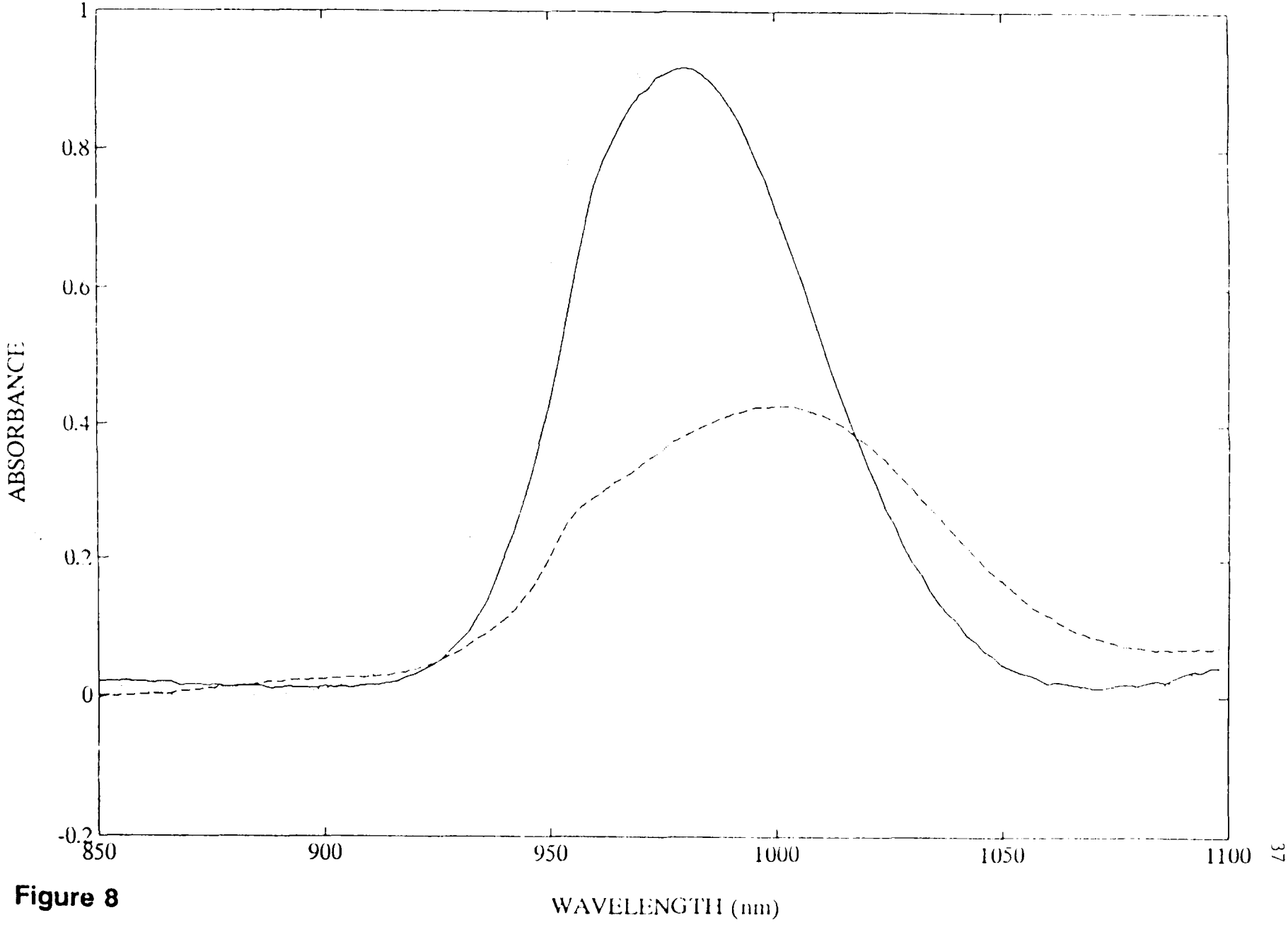
1
0.8
0.6
0.4
0.2
0
-0.2
ABSORBANCE
850
900
950
1000
1050
1100
WAVELENGTH (nm)

Figure 8

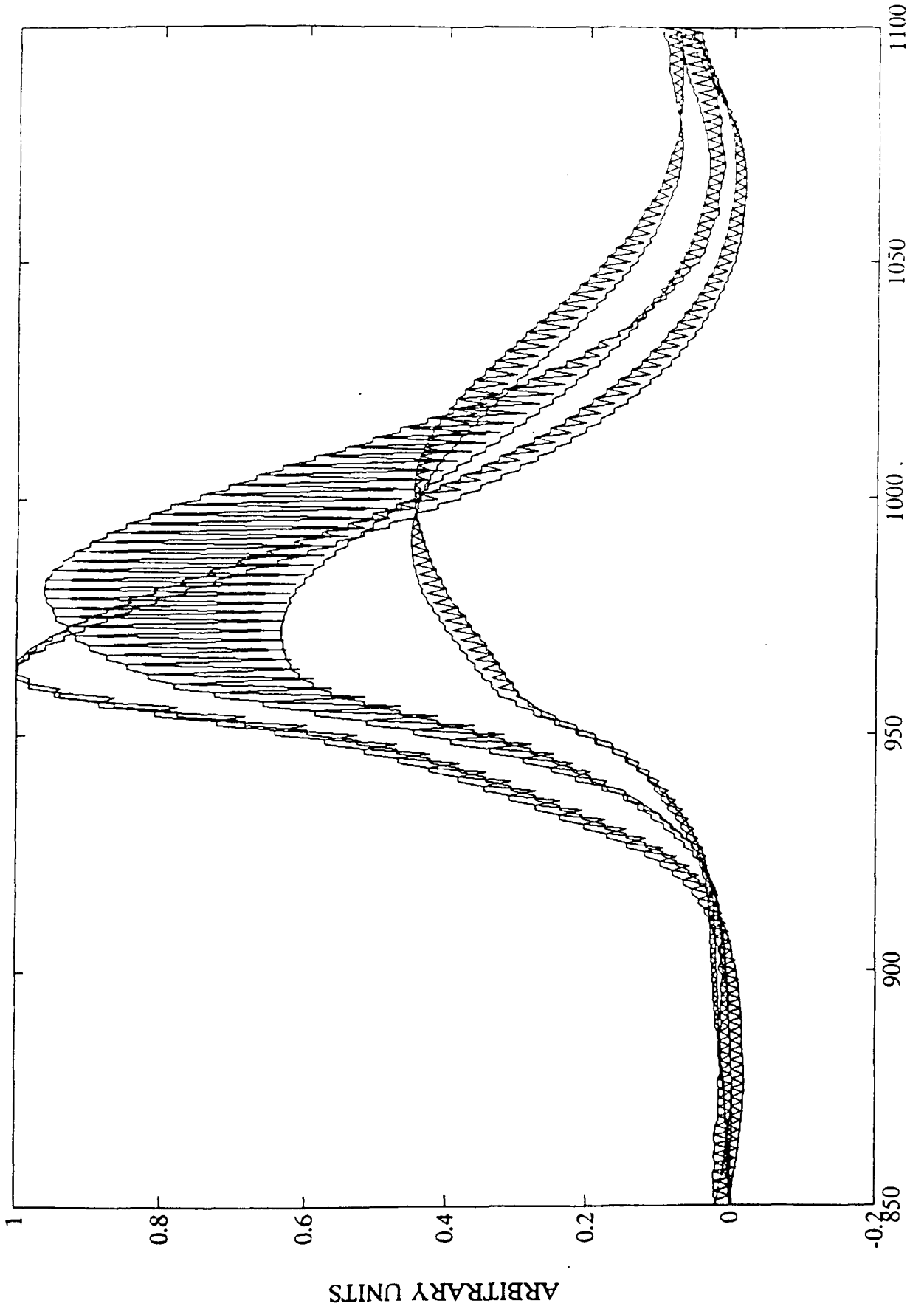
ARBITRARY UNITS
1
0.8
0.6
0.4
0.2
0
-0.2
850
900
950
1000
1050
1100
WAVELENGTH(nm)

Figure 9

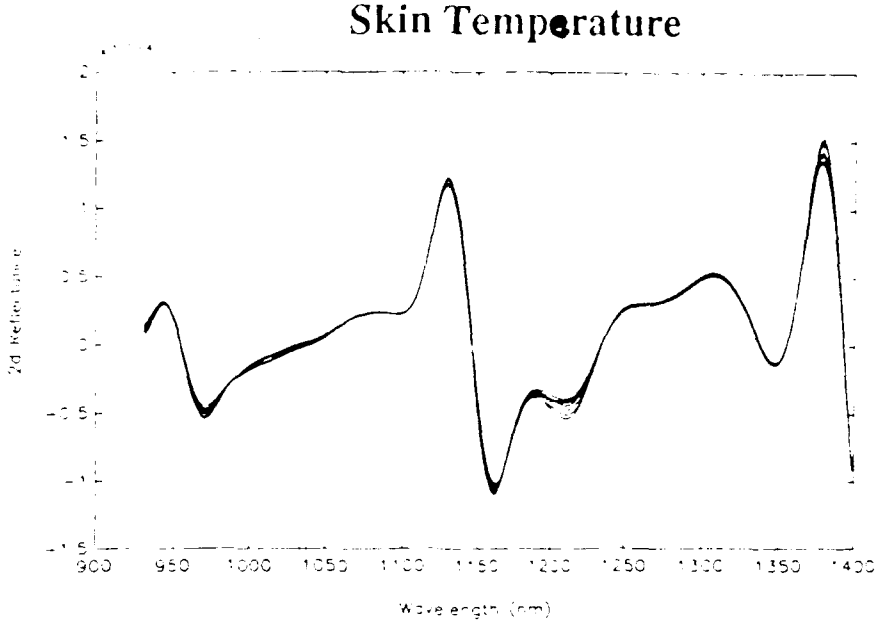

Figure 10

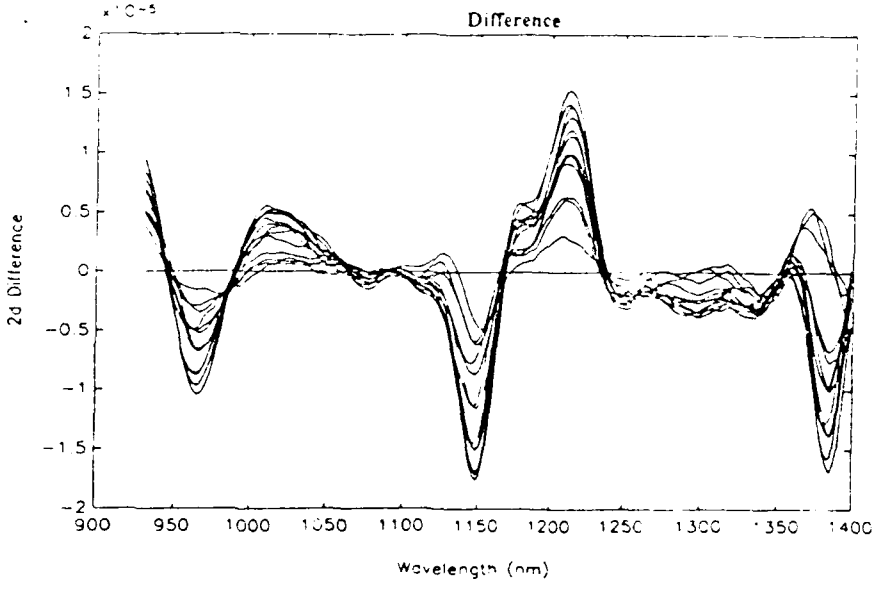

Figure 11

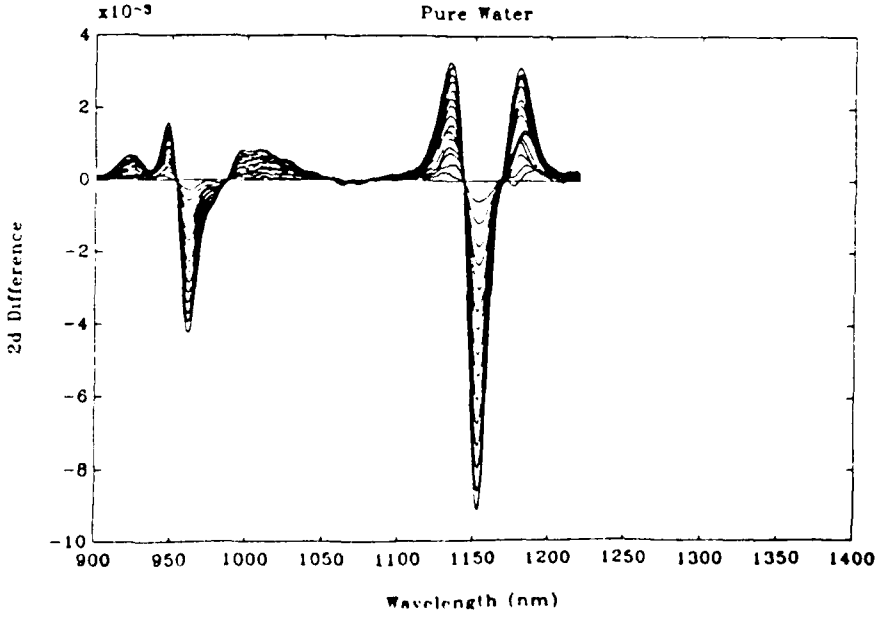

Figure 12

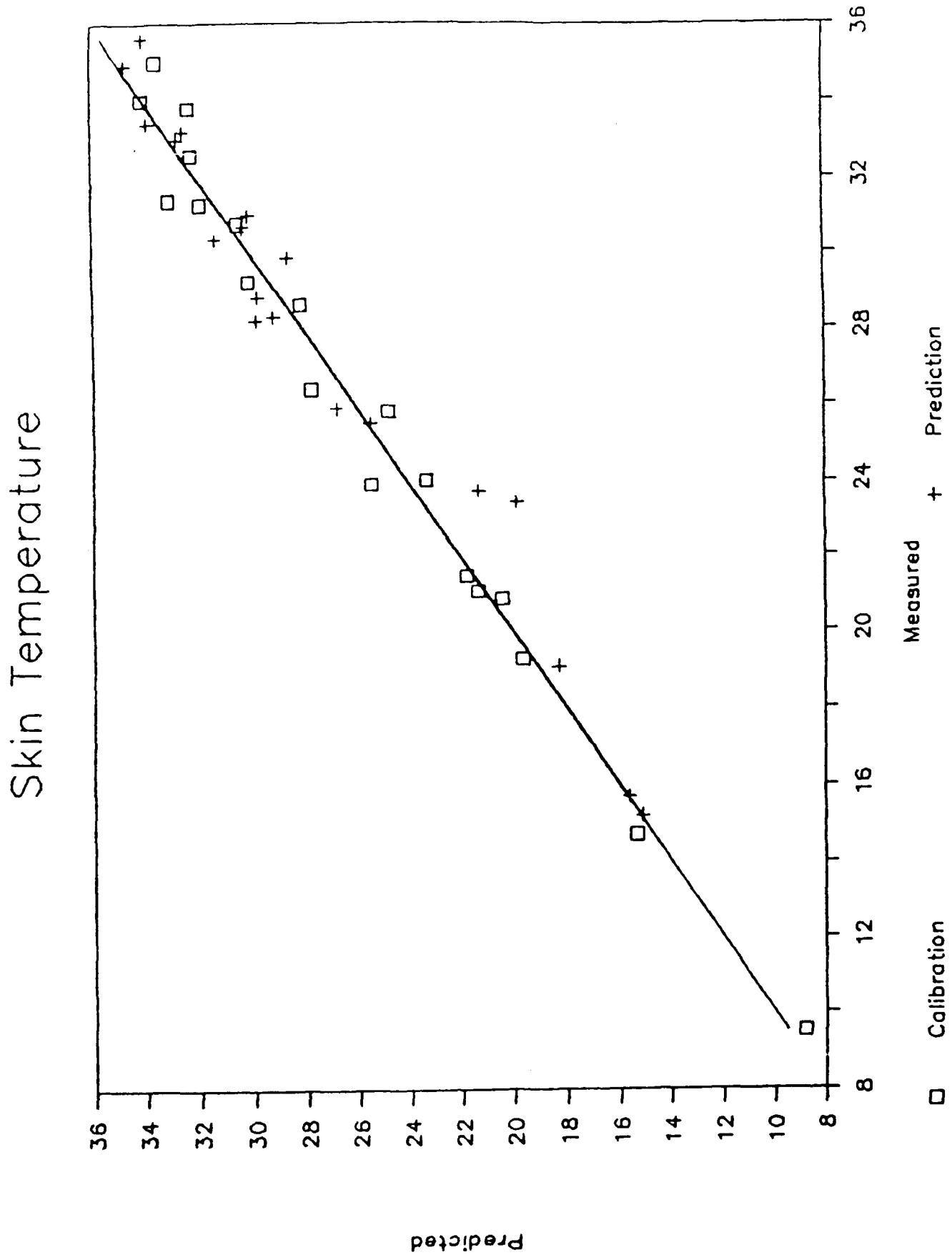
Skin Temperature
Predicted
Measured
Calibration
Prediction
36
34
32
30
28
26
24
22
20
18
16
14
12
10
8
8
12
16
20
24
28
32
36

Figure 13

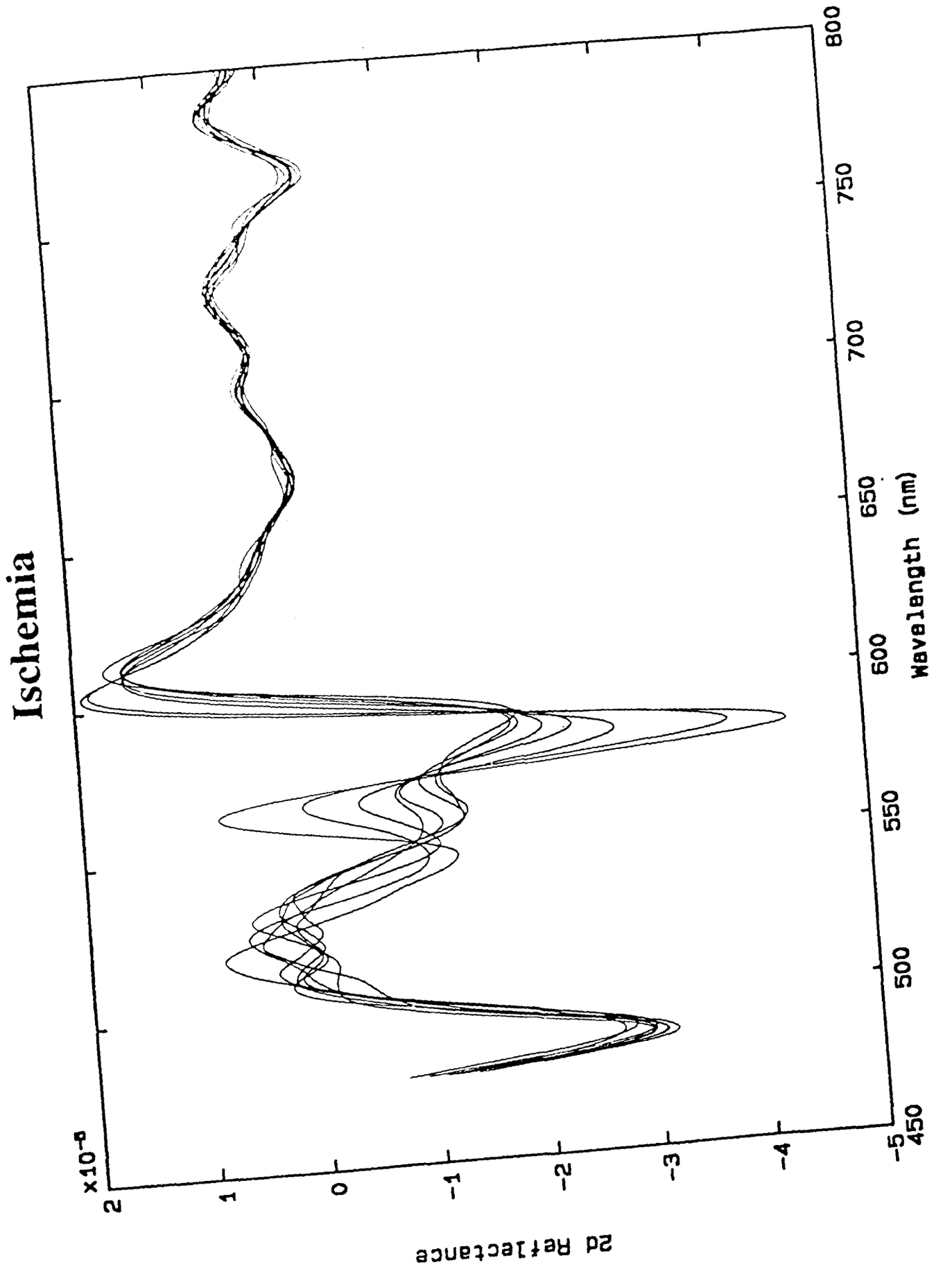
Ischemia
2d Reflectance
x10⁻⁶
2
1
0
-1
-2
-3
-4
-5
450
500
550
600
650
700
750
800
Wavelength (nm)

Figure 14

PCA of Ischemia

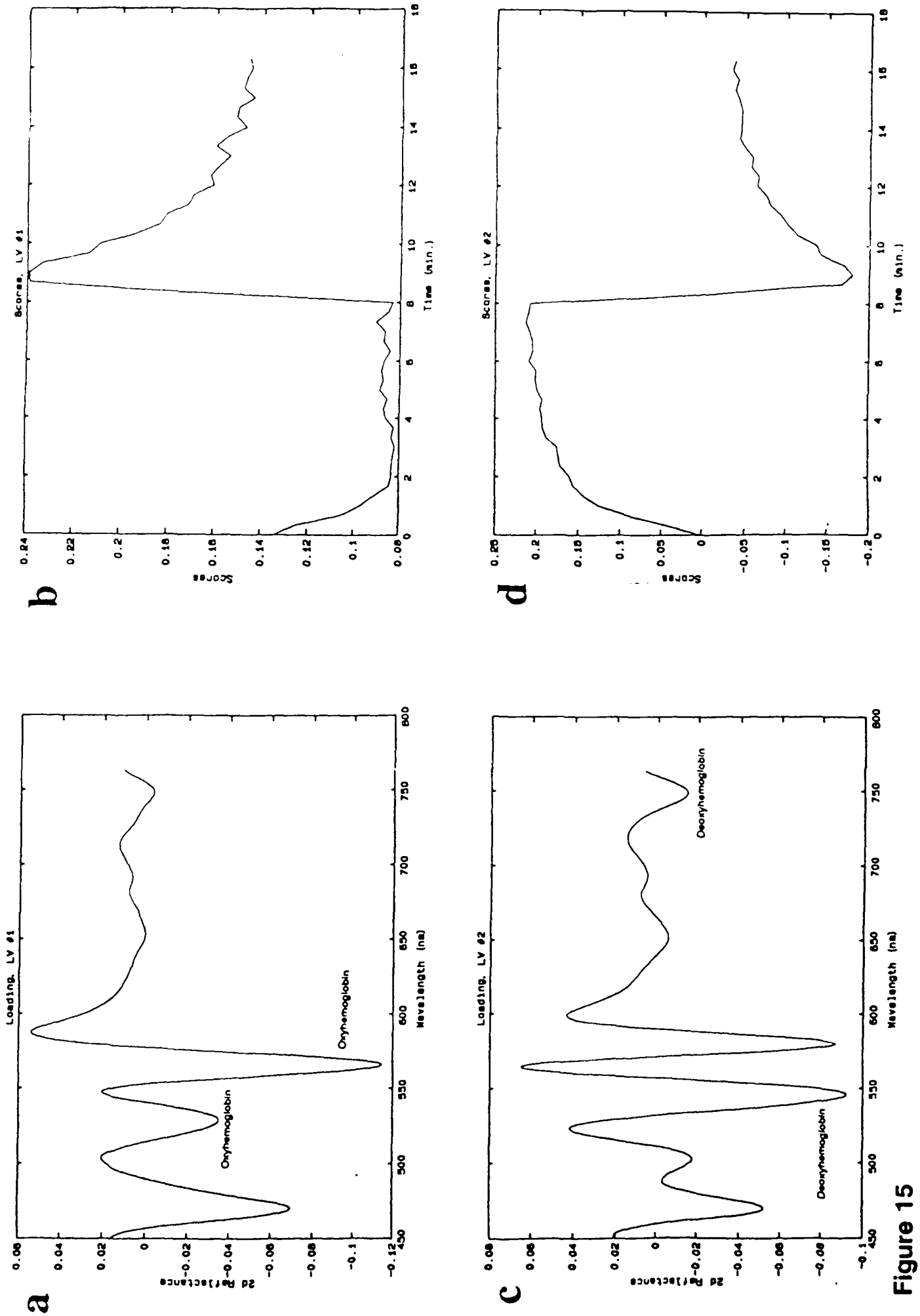

Figure 15

Shallow Burn, Visible

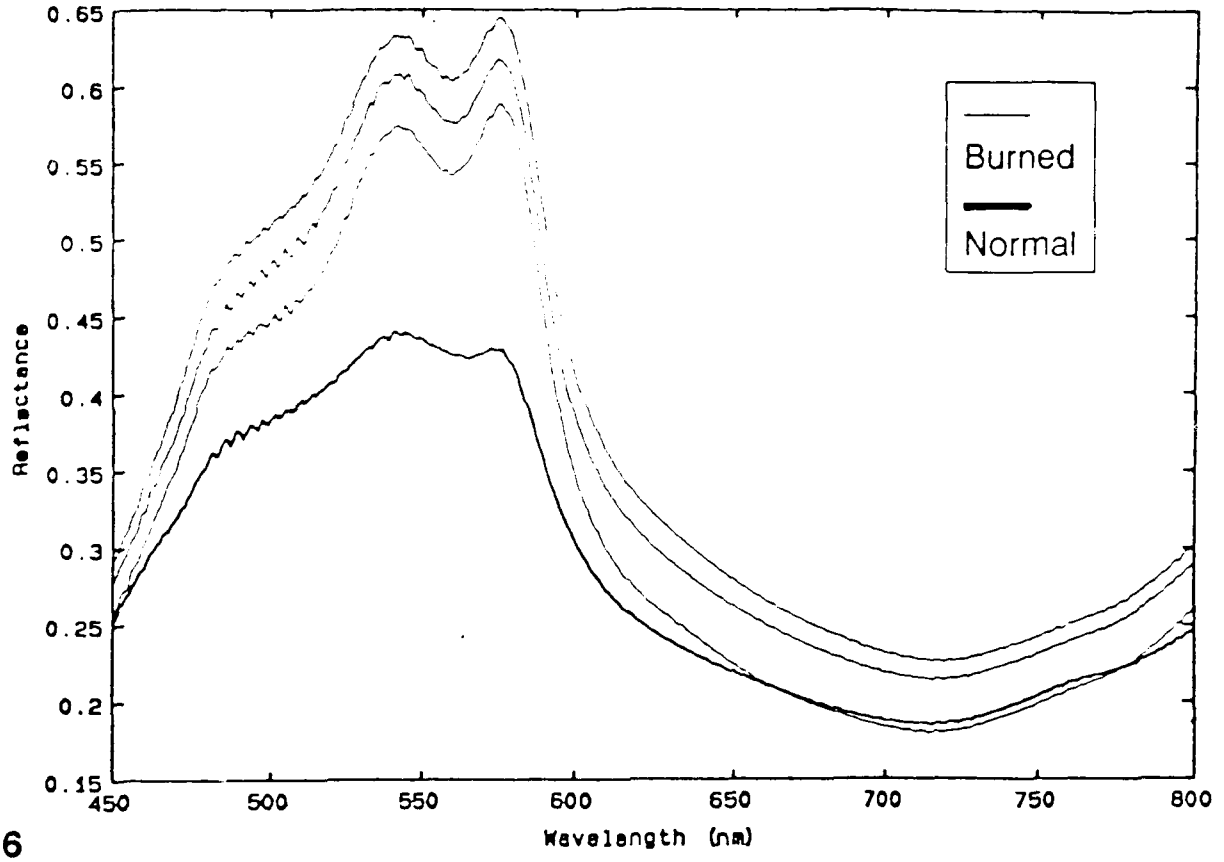

Figure 16

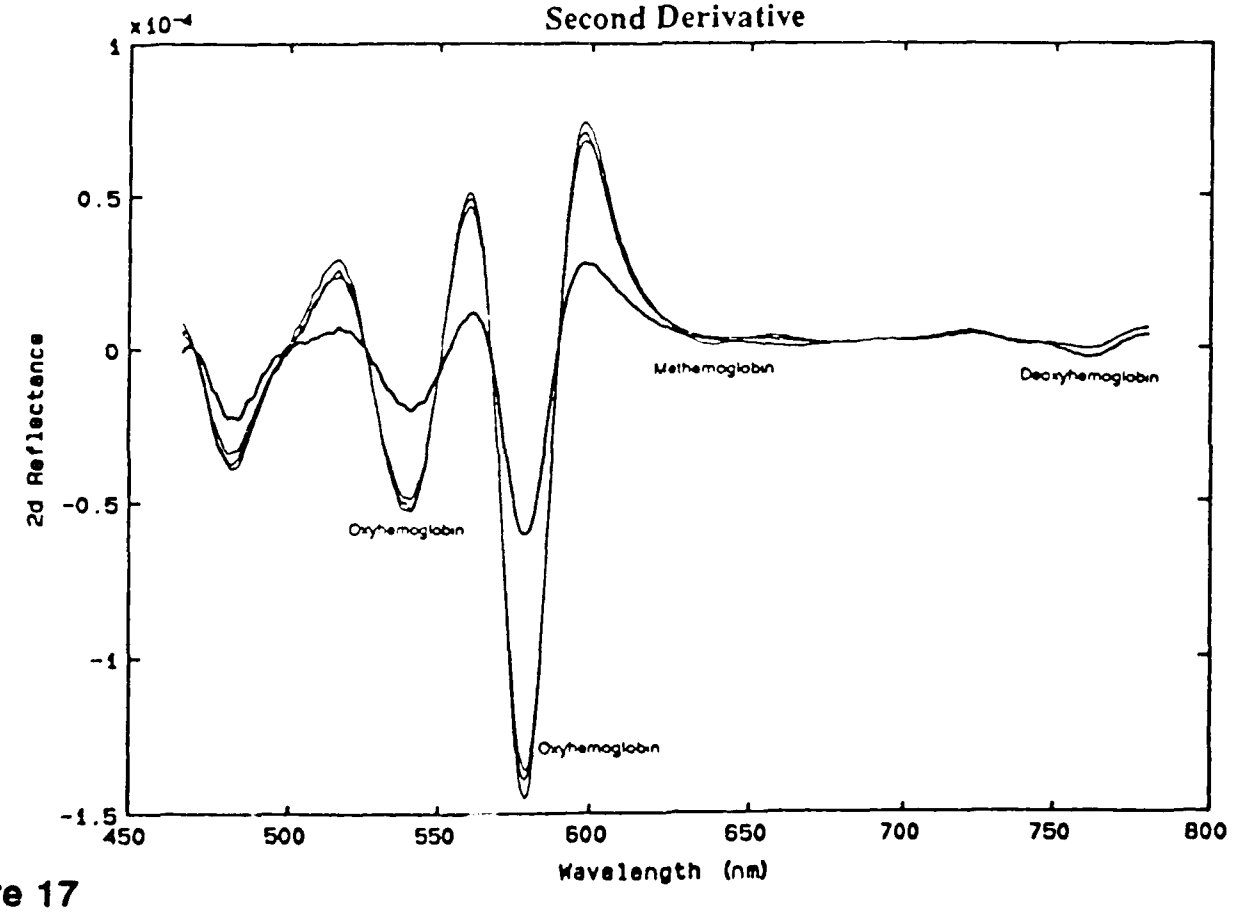

Figure 17

Shallow Burn, NIR

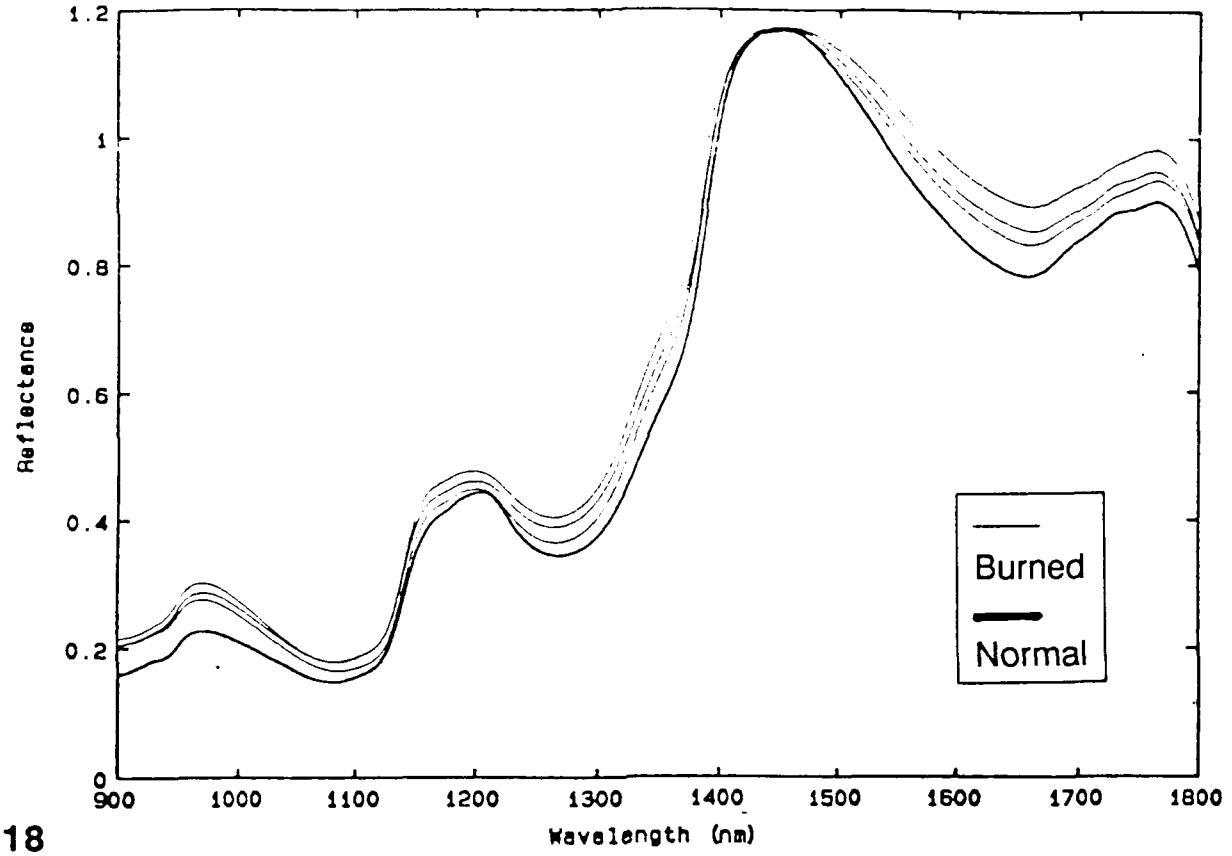

Figure 18

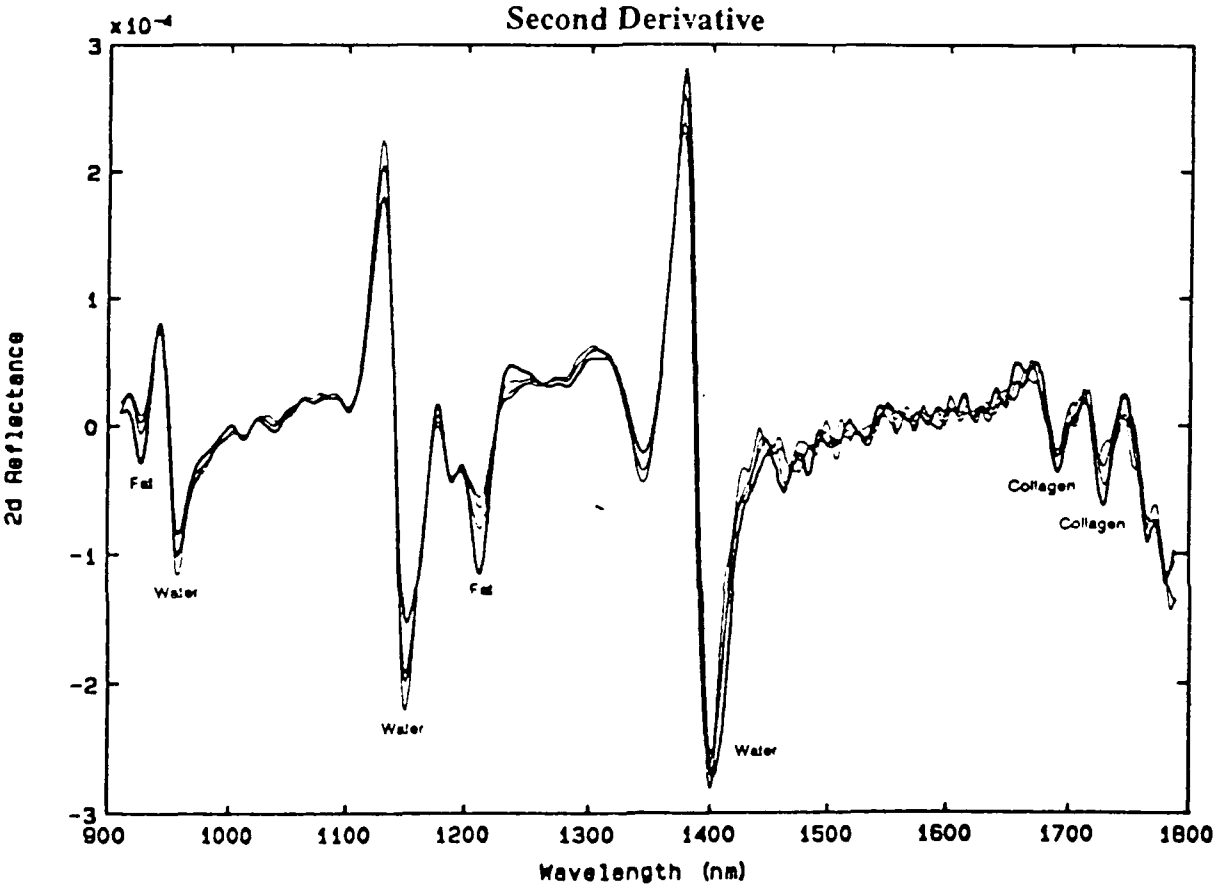

Figure 19

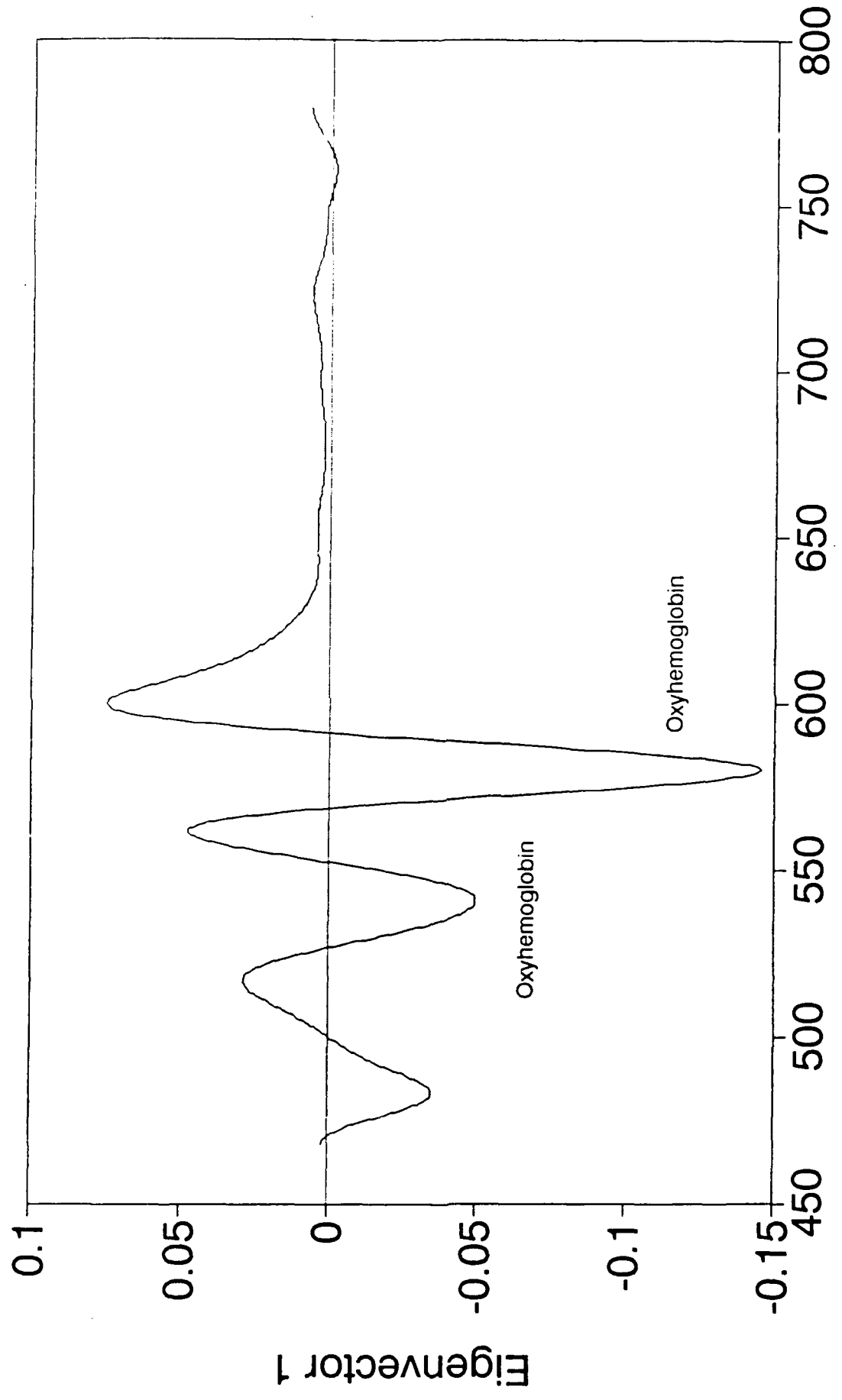
PCA of Shallow Burn
Loading
Eigenvector 1
0.1
0.05
0
-0.05
-0.1
-0.15
450
500
550
600
650
700
750
800
Wavelength
Oxyhemoglobin
Oxyhemoglobin

Figure 20

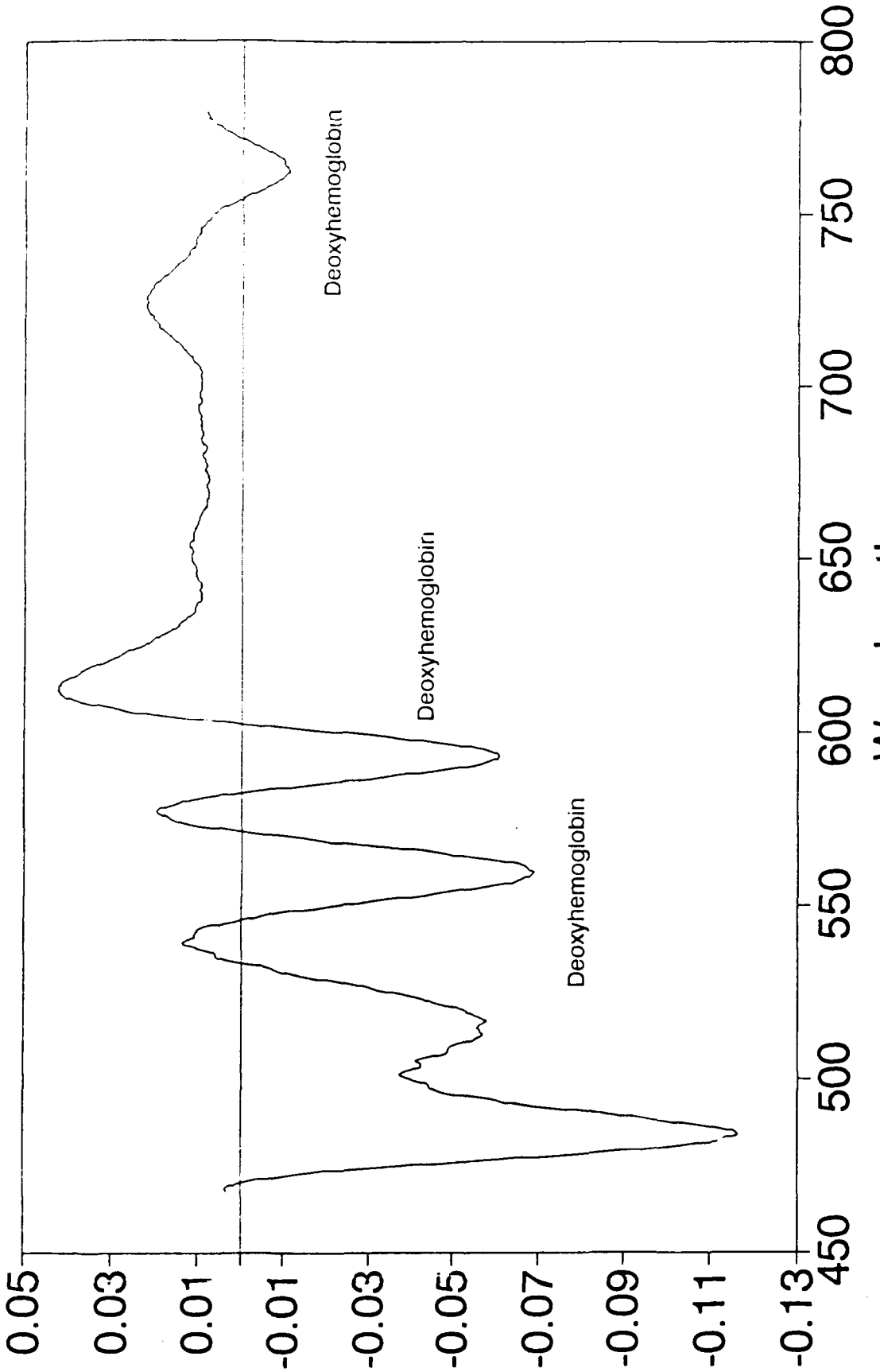
PCA of Shallow Burn
Loading
Eigenvector 2
0.05
0.03
0.01
-0.01
-0.03
-0.05
-0.07
-0.09
-0.11
-0.13
450
500
550
600
650
700
750
800
Wavelength
Deoxyhemoglobin
Deoxyhemoglobin
Deoxyhemoglobin

Figure 21

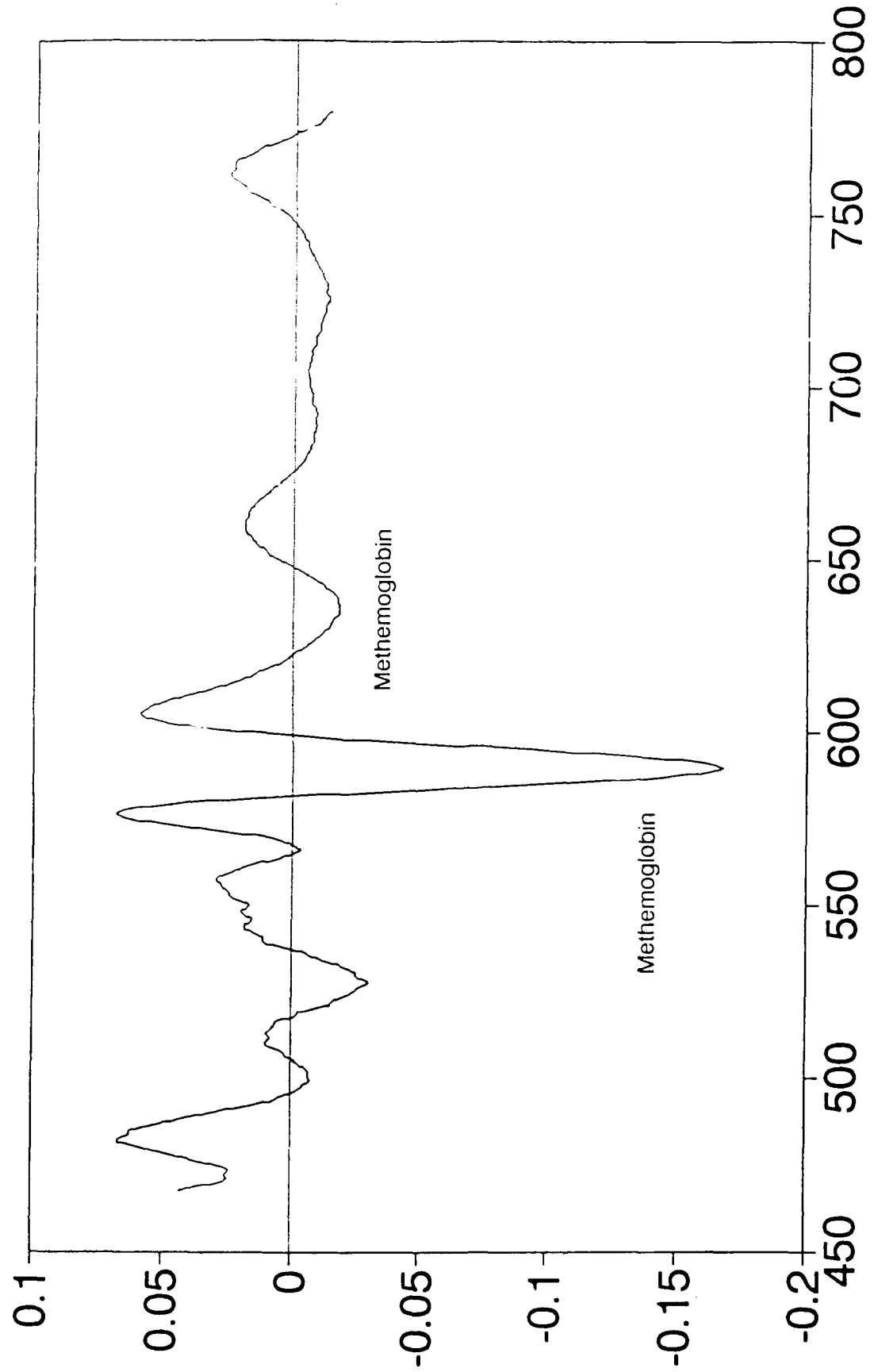
PCA of Shallow Burn
Loading
Eigenvector 3
0.1
0.05
0
-0.05
-0.1
-0.15
-0.2
450
500
550
600
650
700
750
800
Wavelength
Methemoglobin
Methemoglobin

Figure 22

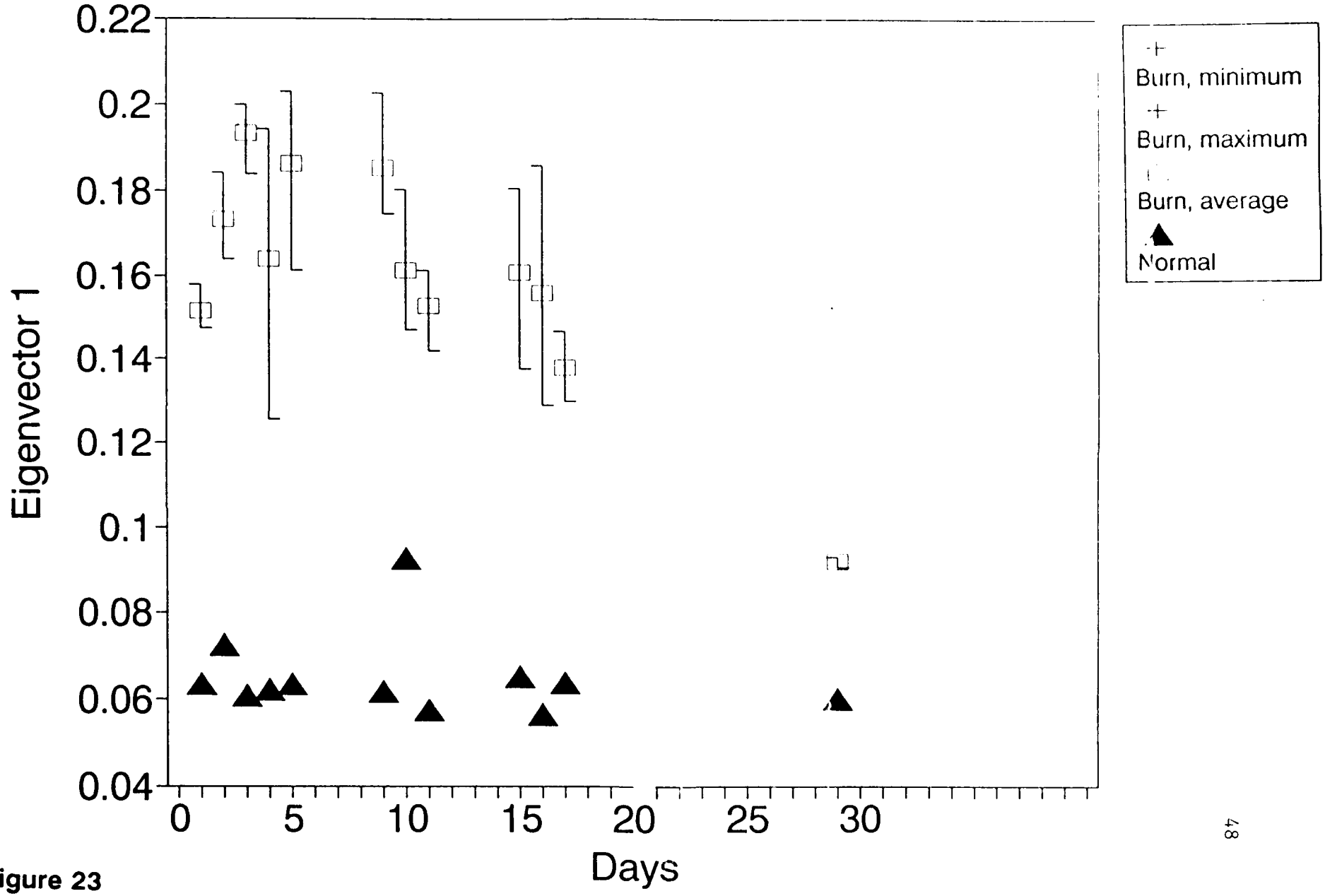
PCA of Shallow Burn
Scores
Eigenvector 1
0.22
0.2
0.18
0.16
0.14
0.12
0.1
0.08
0.06
0.04
0
5
10
15
20
25
30
Days
Burn, minimum
Burn, maximum
Burn, average
Normal

Figure 23

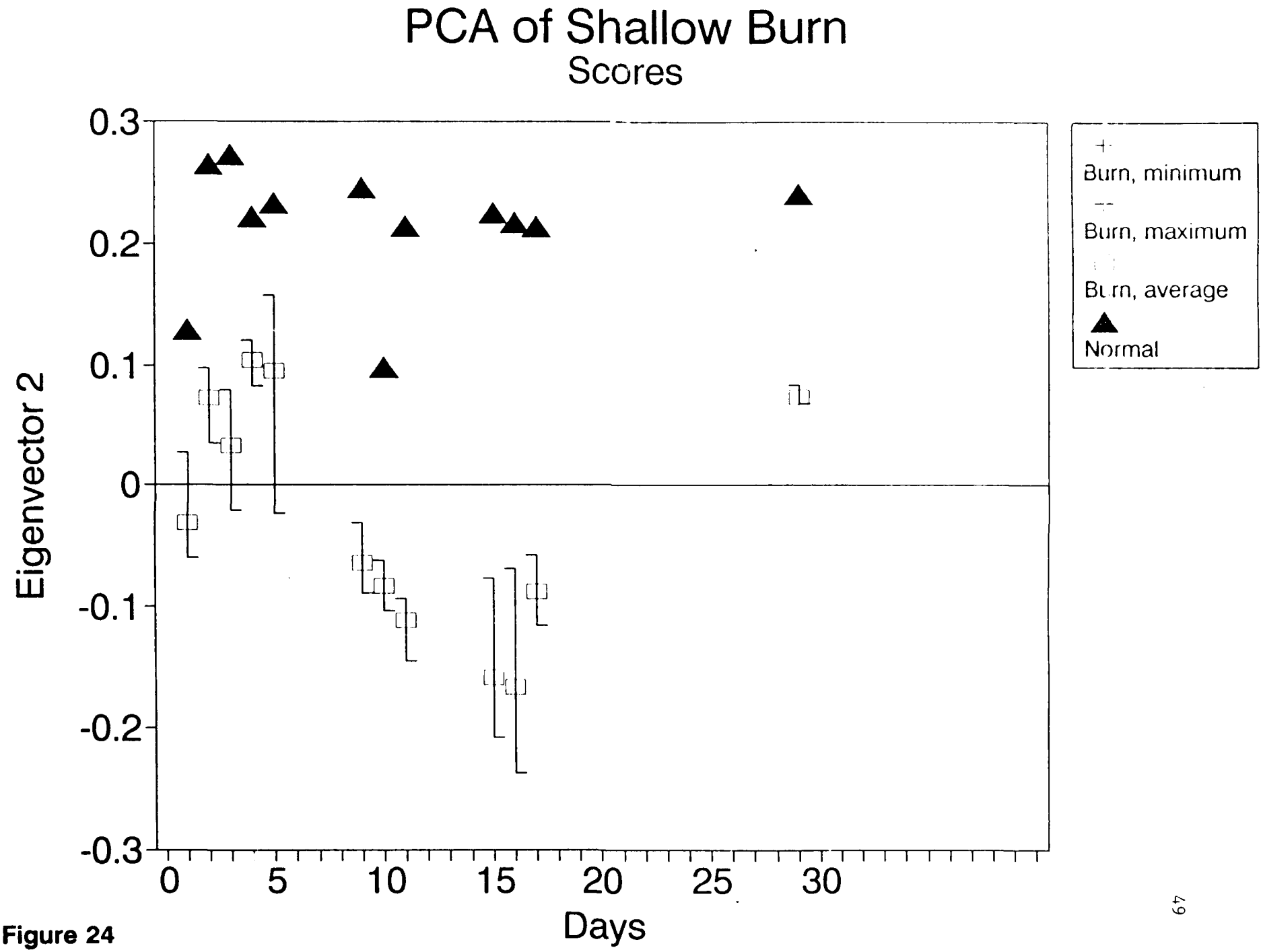
PCA of Shallow Burn
Scores
0.3
0.2
0.1
0
-0.1
-0.2
-0.3
Eigenvector 2
0
5
10
15
20
25
30
Days
Burn, minimum
Burn, maximum
Burn, average
Normal

Figure 24

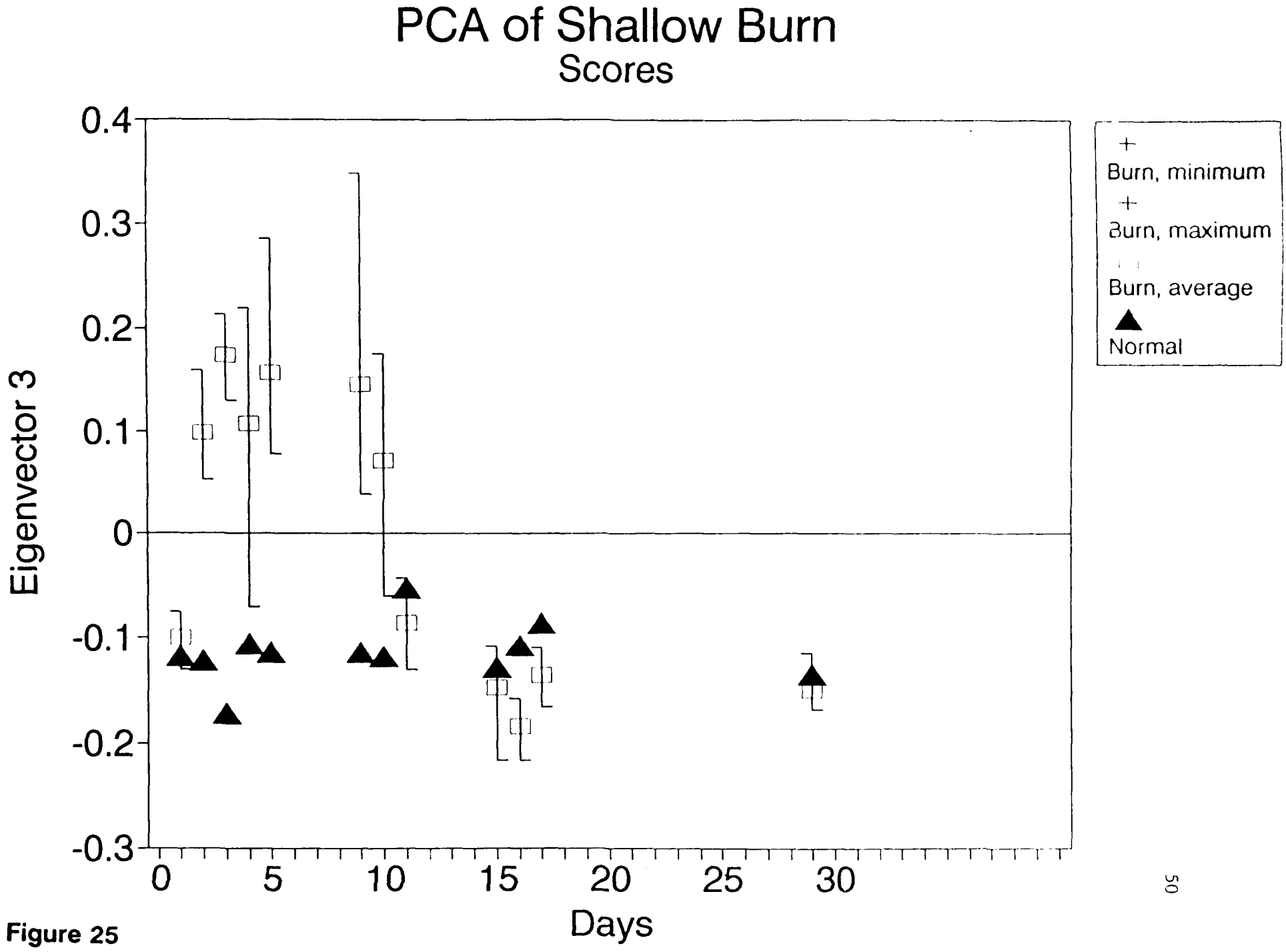
PCA of Shallow Burn
Scores
0.4
0.3
0.2
0.1
0
-0.1
-0.2
-0.3
Eigenvector 3
0
5
10
15
20
25
30
Days
Burn, minimum
Burn, maximum
Burn, average
Normal

Figure 25

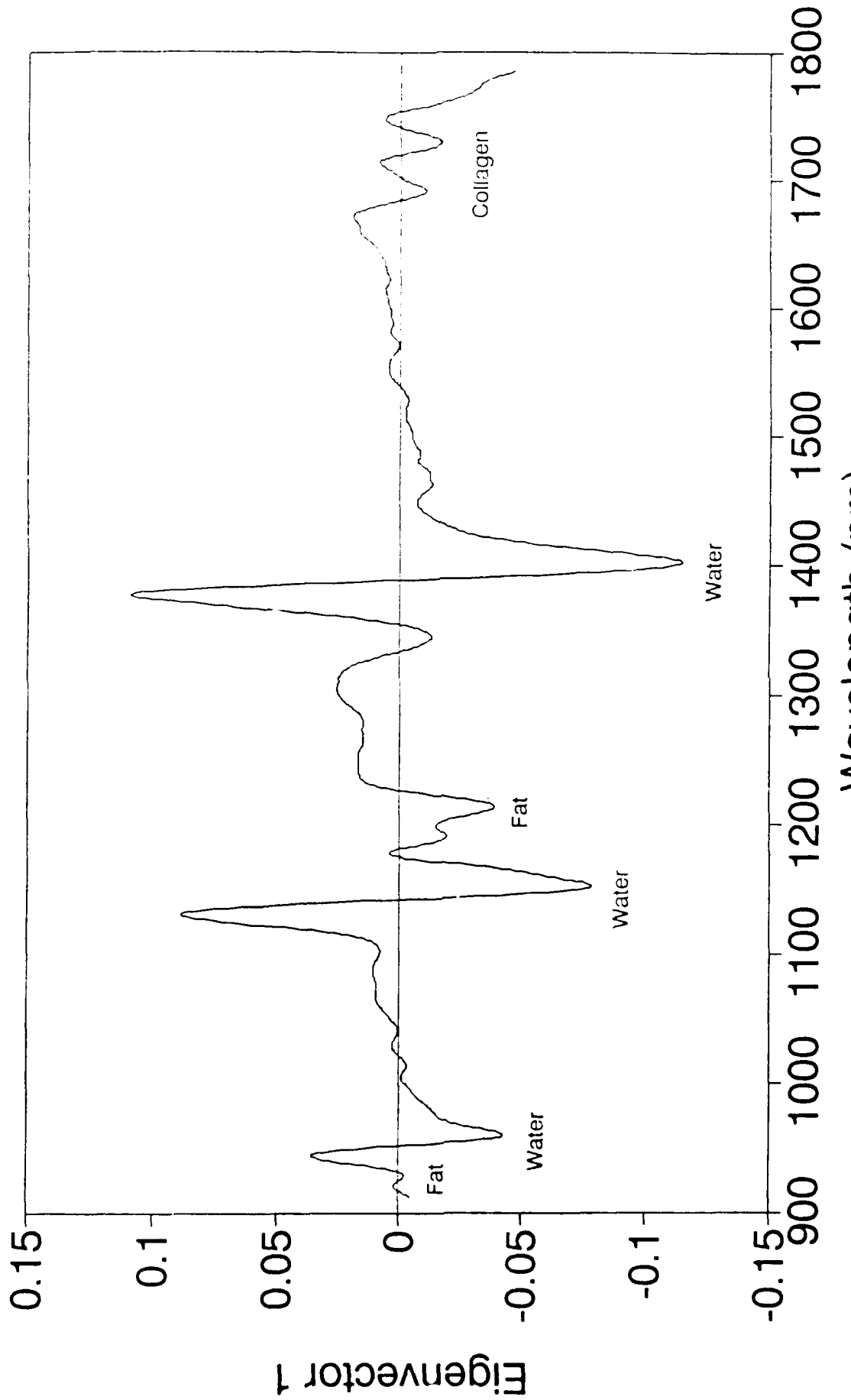
PCA of Shallow Burn
Loading, NIR
Eigenvector 1
0.15
0.1
0.05
0
-0.05
-0.1
-0.15
900
1000
1100
1200
1300
1400
1500
1600
1700
1800
Wavelength (nm)
Fat
Water
Water
Fat
Water
Collagen

Figure 26

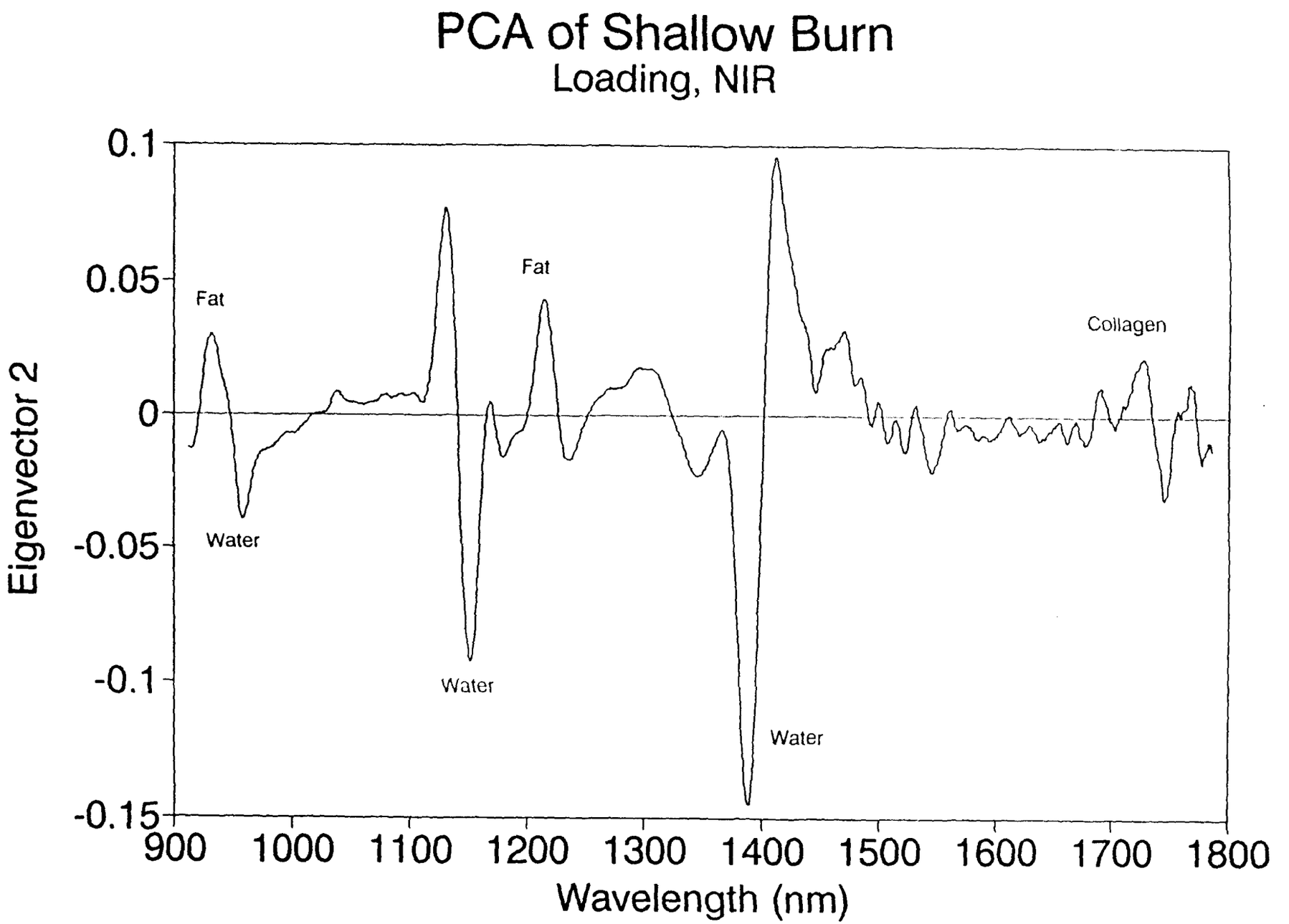
PCA of Shallow Burn
Loading, NIR
0.1
0.05
0
-0.05
-0.1
-0.15
Eigenvector 2
Fat
Water
Fat
Water
Water
Collagen
900
1000
1100
1200
1300
1400
1500
1600
1700
1800
Wavelength (nm)

Figure 27

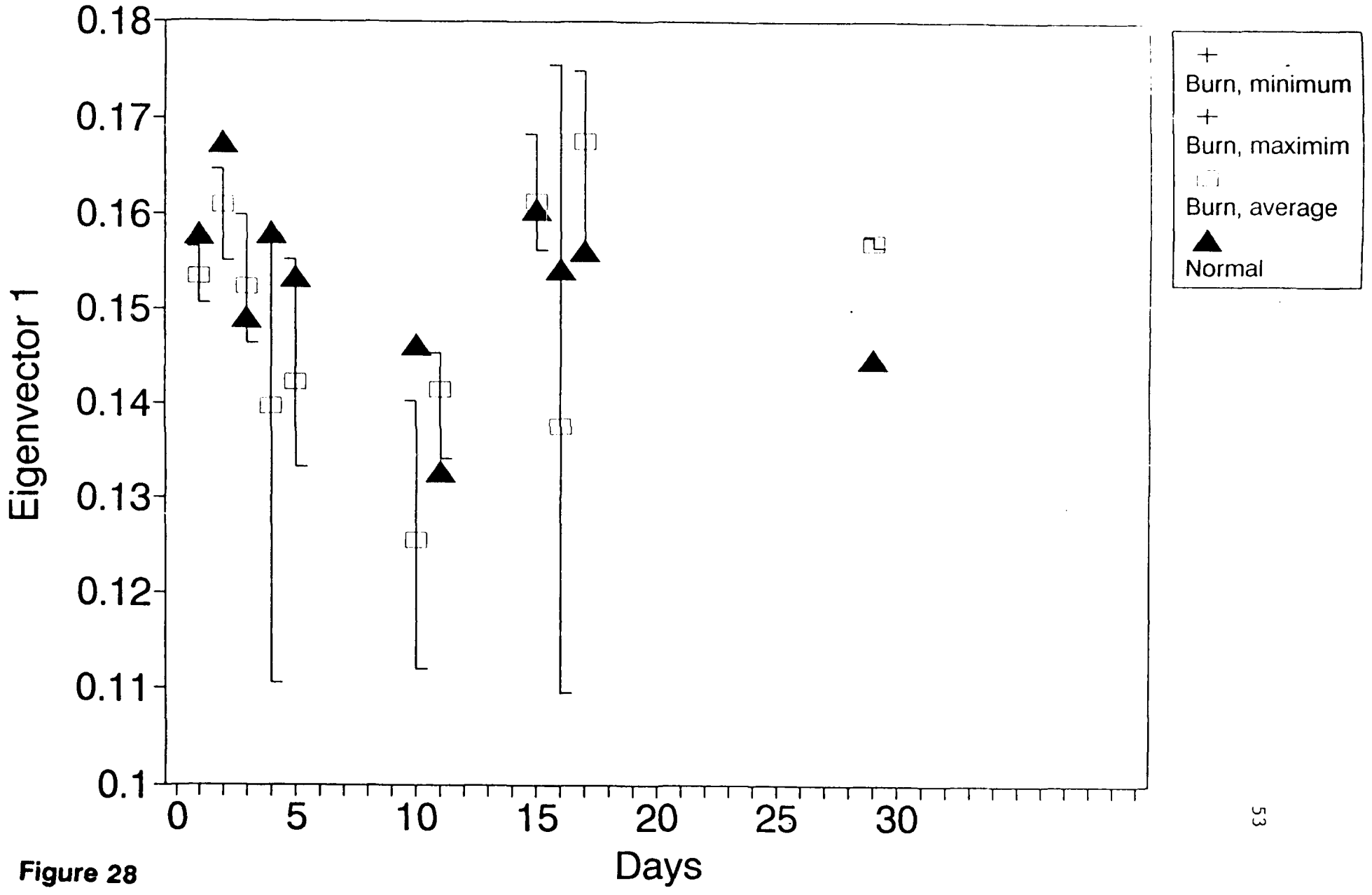
PCA of Shallow Burn
Scores, NIR
Eigenvector 1
0.18
0.17
0.16
0.15
0.14
0.13
0.12
0.11
0.1
0
5
10
15
20
25
30
Days
Burn, minimum
Burn, maximim
Burn, average
Normal

Figure 28

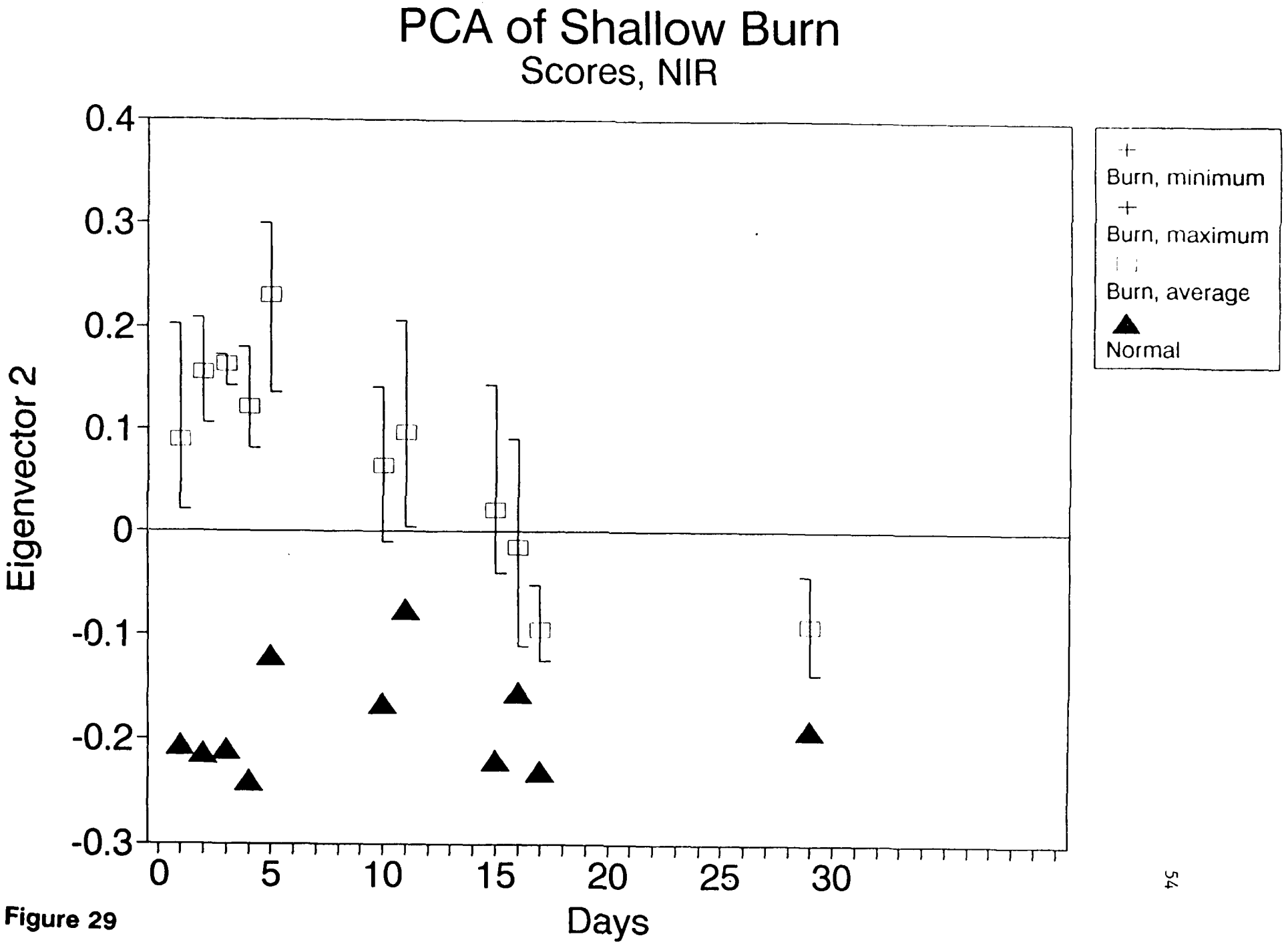
PCA of Shallow Burn
Scores, NIR
Eigenvector 2
0.4
0.3
0.2
0.1
0
-0.1
-0.2
-0.3
0
5
10
15
20
25
30
Days
Burn, minimum
Burn, maximum
Burn, average
Normal

Figure 29

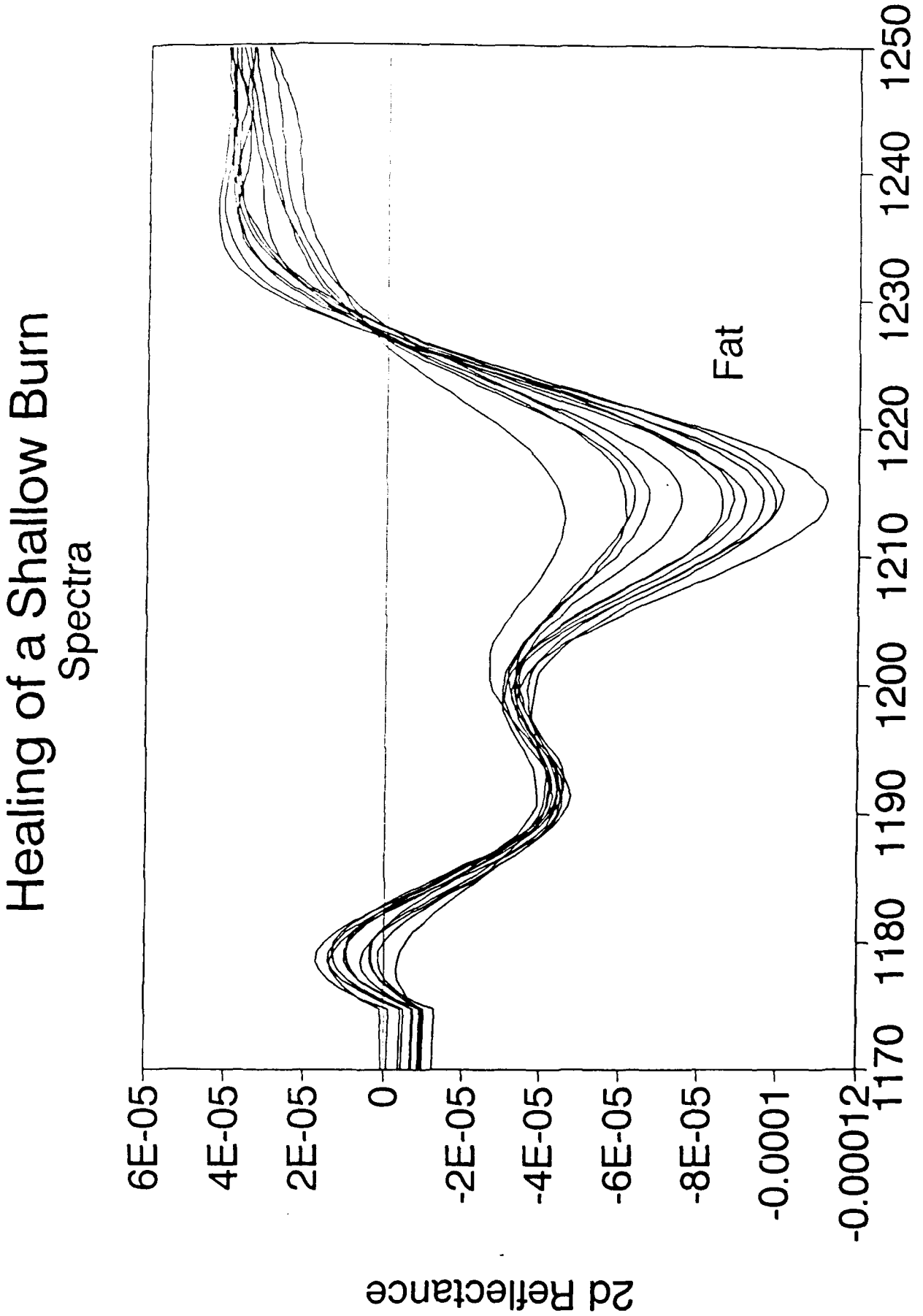
Healing of a Shallow Burn
Spectra
2d Reflectance
6E-05
4E-05
2E-05
0
-2E-05
-4E-05
-6E-05
-8E-05
-0.0001
-0.00012
1170
1180
1190
1200
1210
1220
1230
1240
1250
Wavelength (nm)
Fat

Figure 30

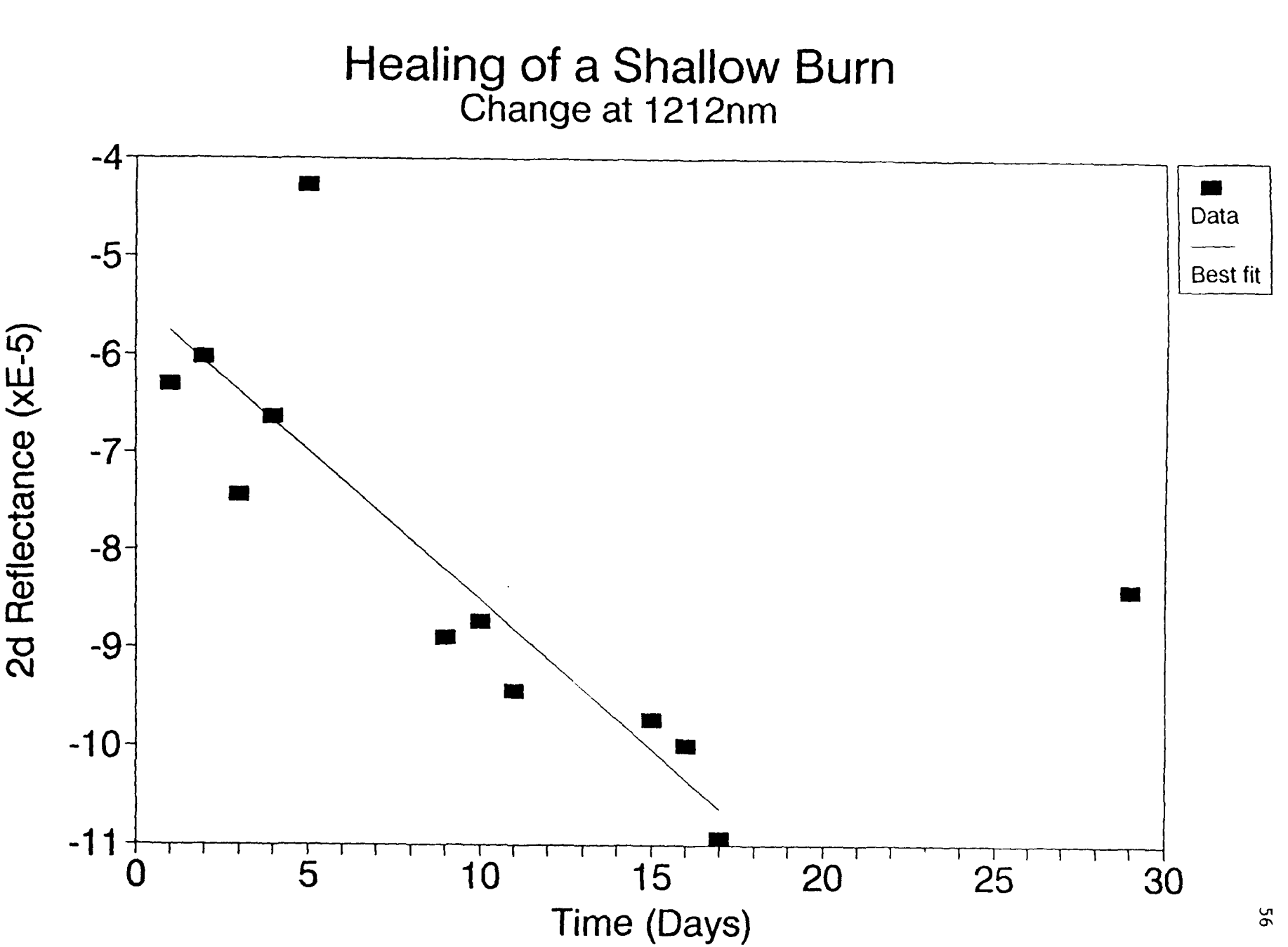
Healing of a Shallow Burn
Change at 1212nm
2d Reflectance (xE-5)
-4
-5
-6
-7
-8
-9
-10
-11
0
5
10
15
20
25
30
Time (Days)
Data
Best fit

Figure 31

Shallow and Deep Burns

Patient 14

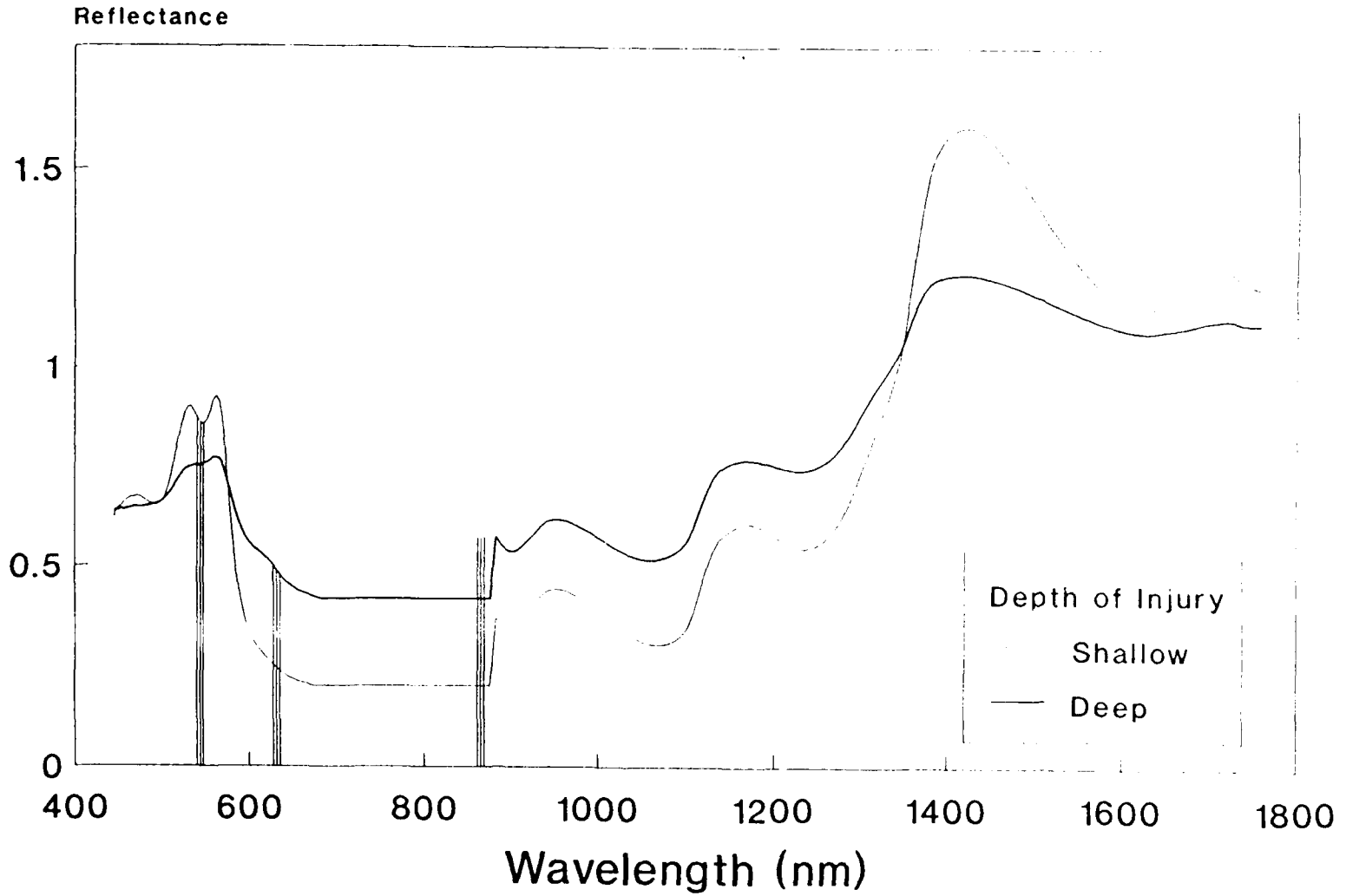

Figure 32

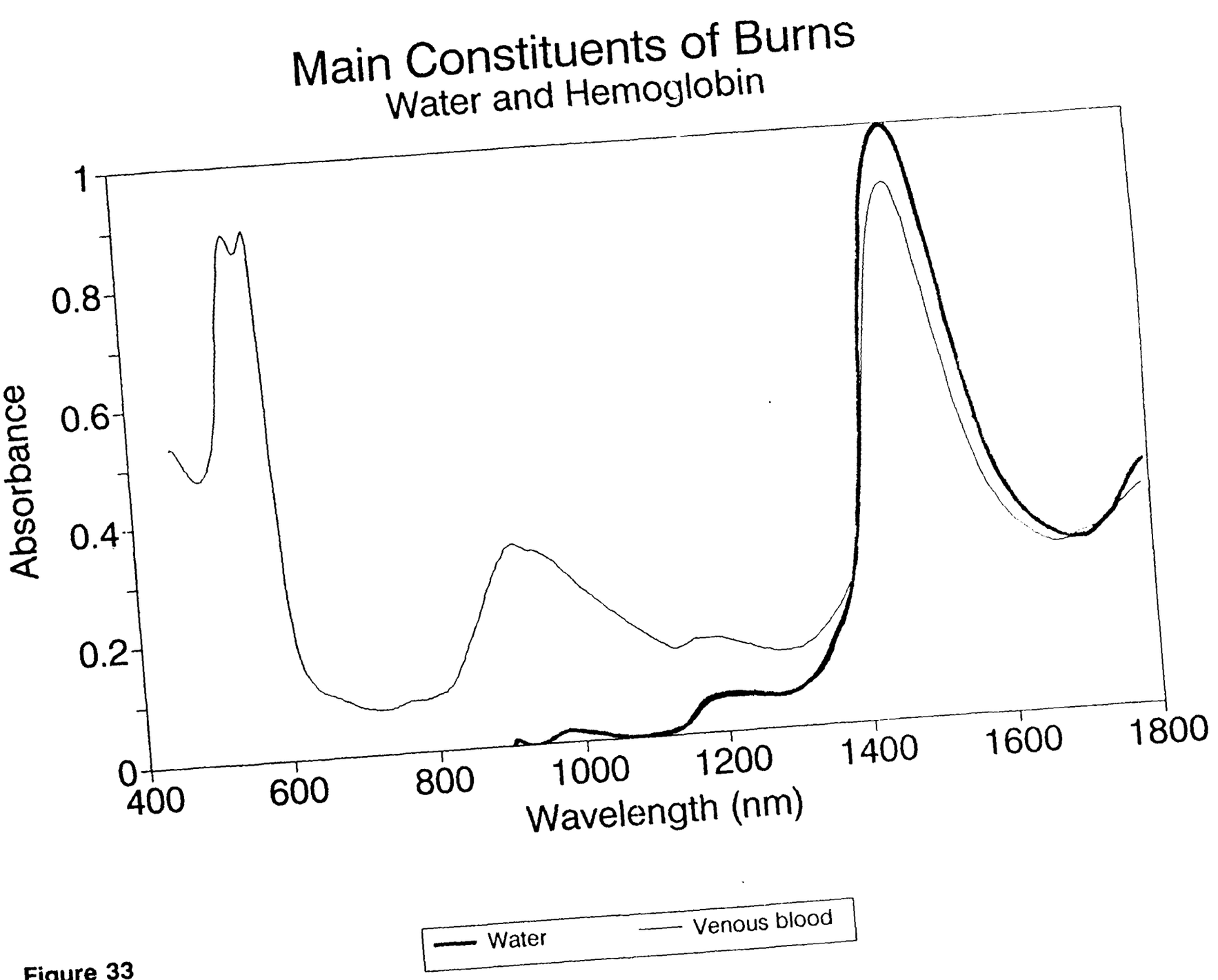
Main Constituents of Burns
Water and Hemoglobin
Absorbance
1
0.8
0.6
0.4
0.2
0
400
600
800
1000
1200
1400
1600
1800
Wavelength (nm)
Water
Venous blood

Figure 33

Indeterminate Burn

Patient 8

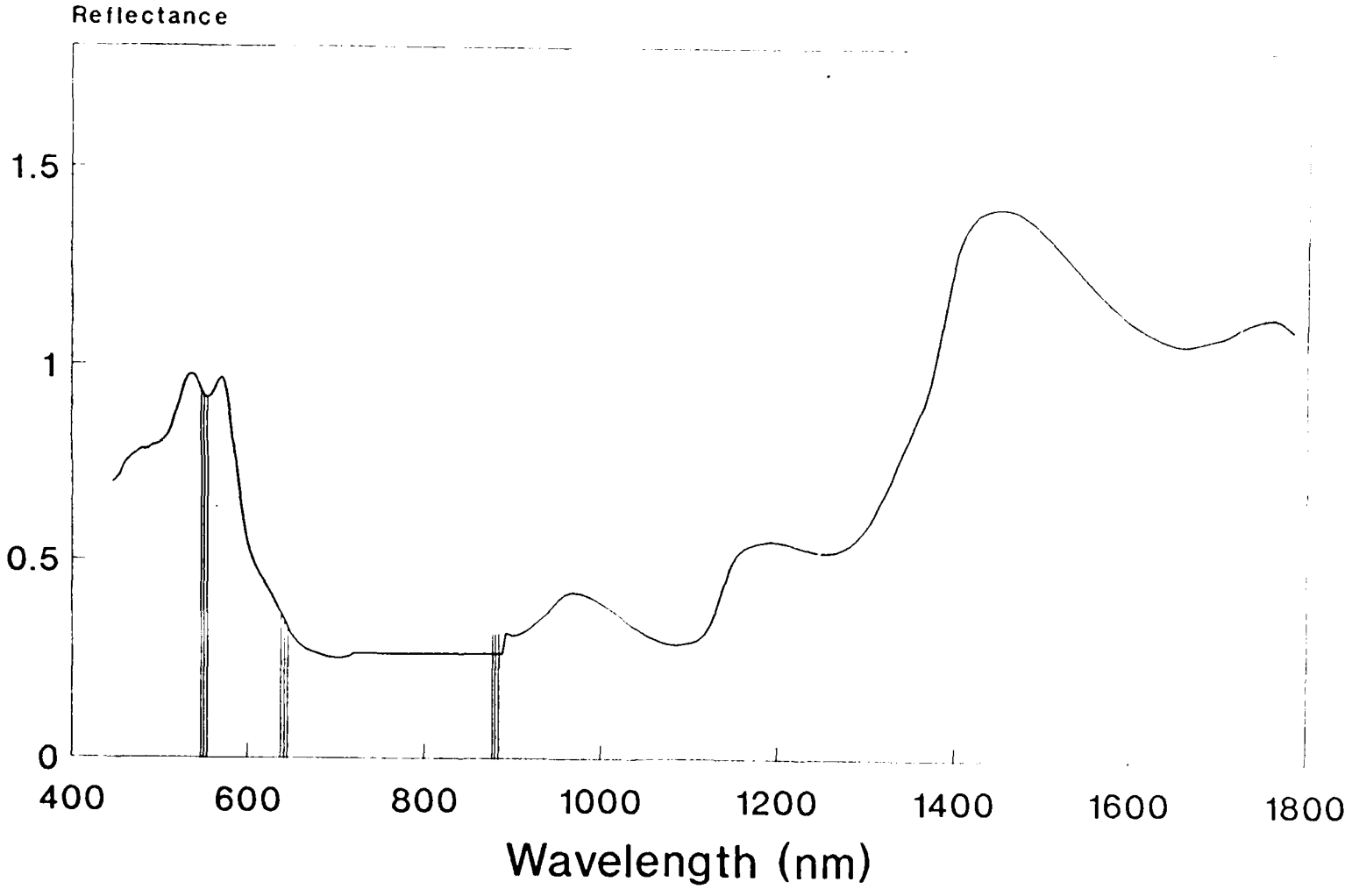

Figure 34

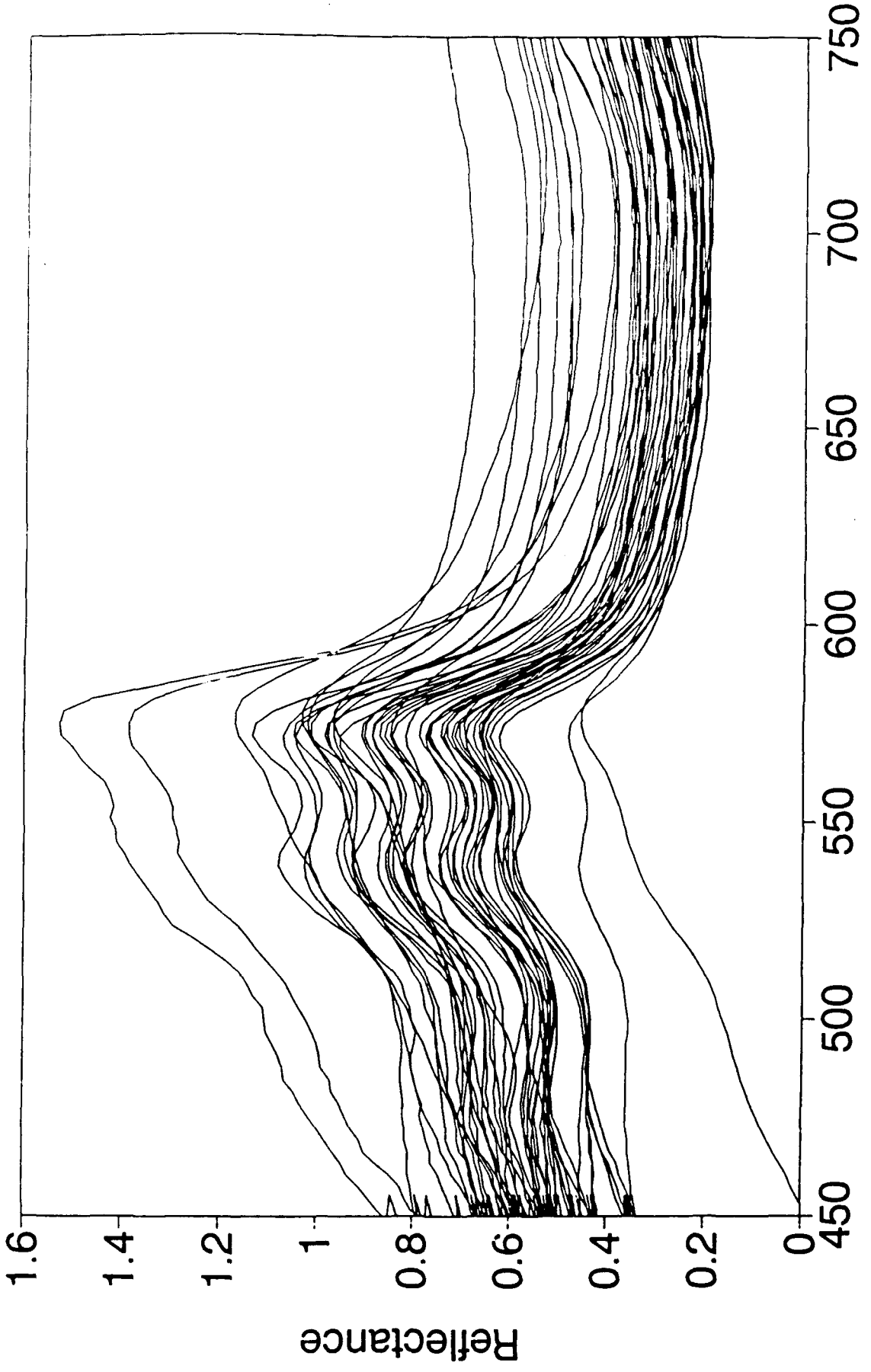
Aggregate Spectra, Visible
Shallow Burns
Reflectance
1.6
1.4
1.2
1
0.8
0.6
0.4
0.2
0
450
500
550
600
650
700
750
Wavelength (nm)

Figure 35

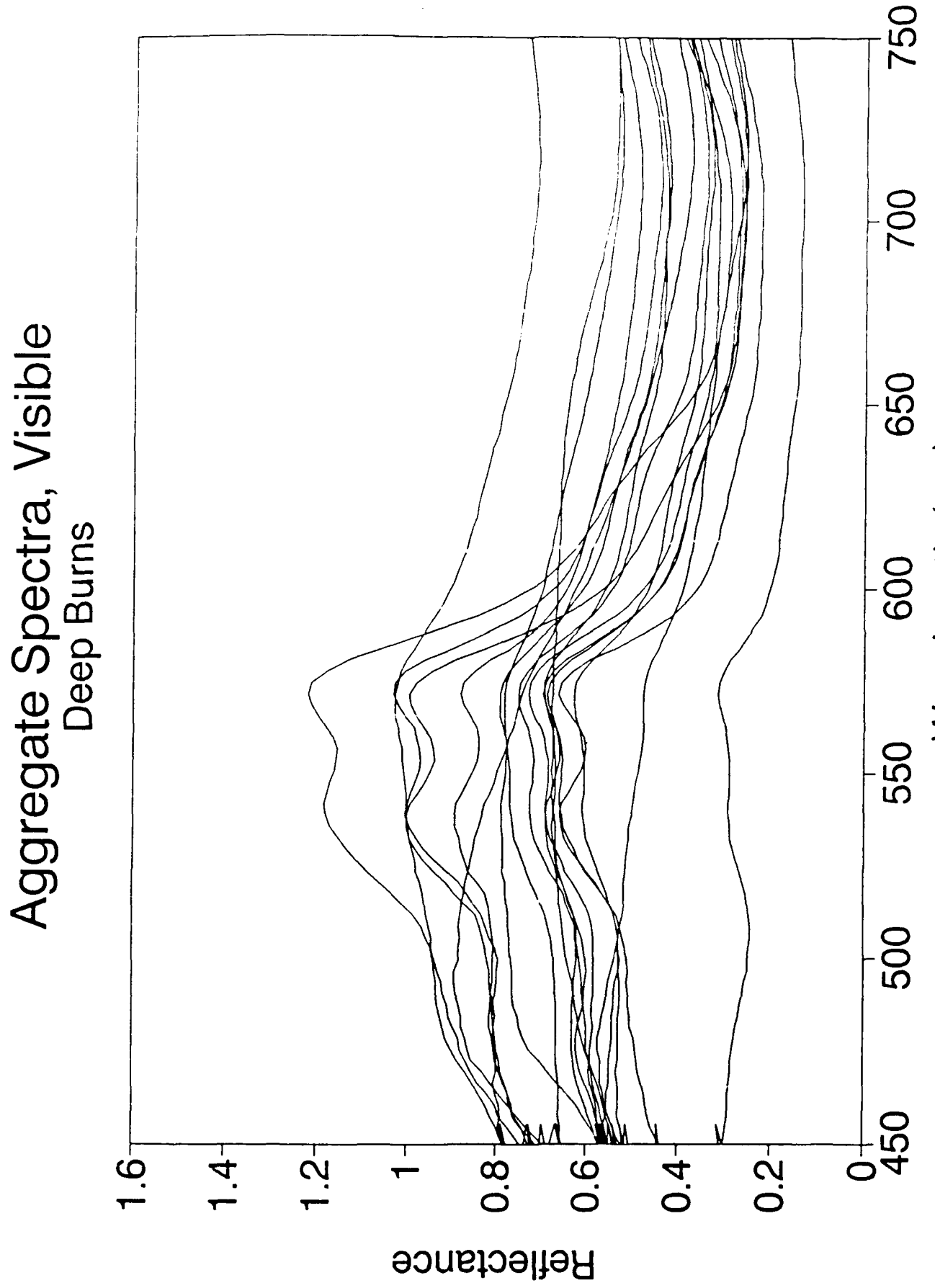
Aggregate Spectra, Visible
Deep Burns
Reflectance
1.6
1.4
1.2
1
0.8
0.6
0.4
0.2
0
450
500
550
600
650
700
750
Wavelength (nm)

Figure 36

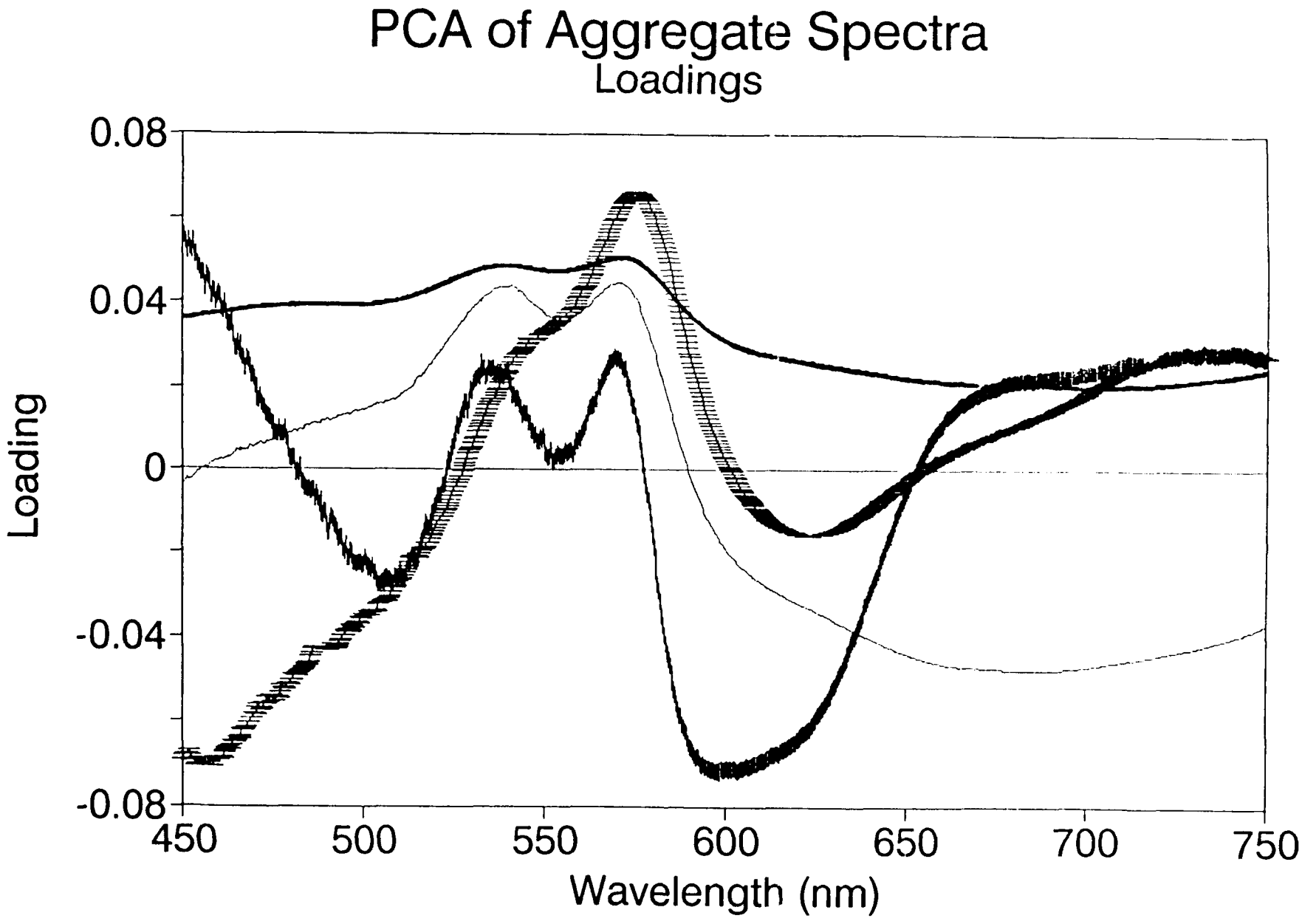
PCA of Aggregate Spectra
Loadings
0.08
0.04
0
-0.04
-0.08
Loading
450
500
550
600
650
700
750
Wavelength (nm)
Eigenvector 1
Eigenvector 2
Eigenvector 3
Eigenvector 4

Figure 37

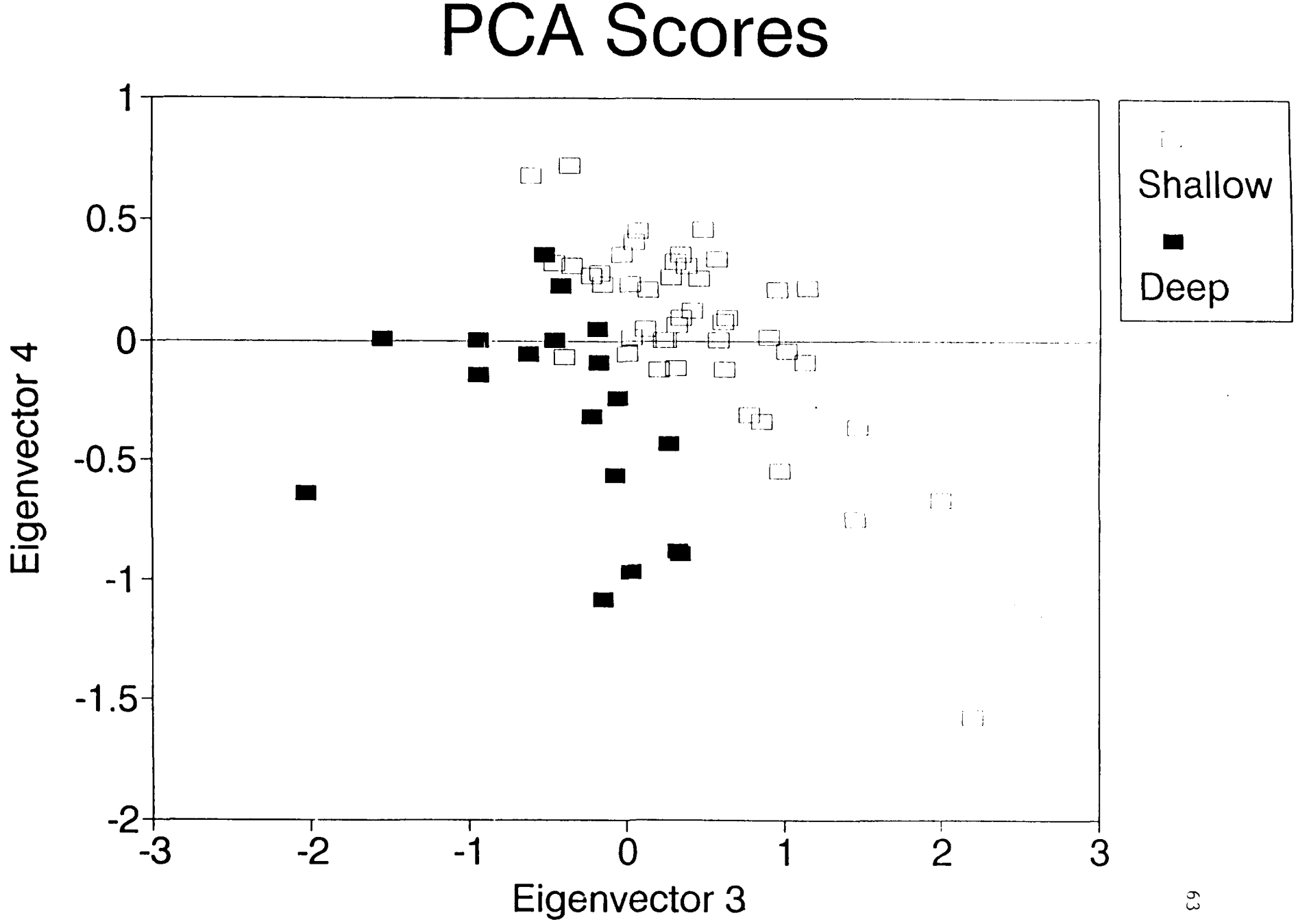
PCA Scores
Shallow
Deep
Eigenvector 4
Eigenvector 3
1
0.5
0
-0.5
-1
-1.5
-2
-3
-2
-1
0
1
2
3

Figure 38

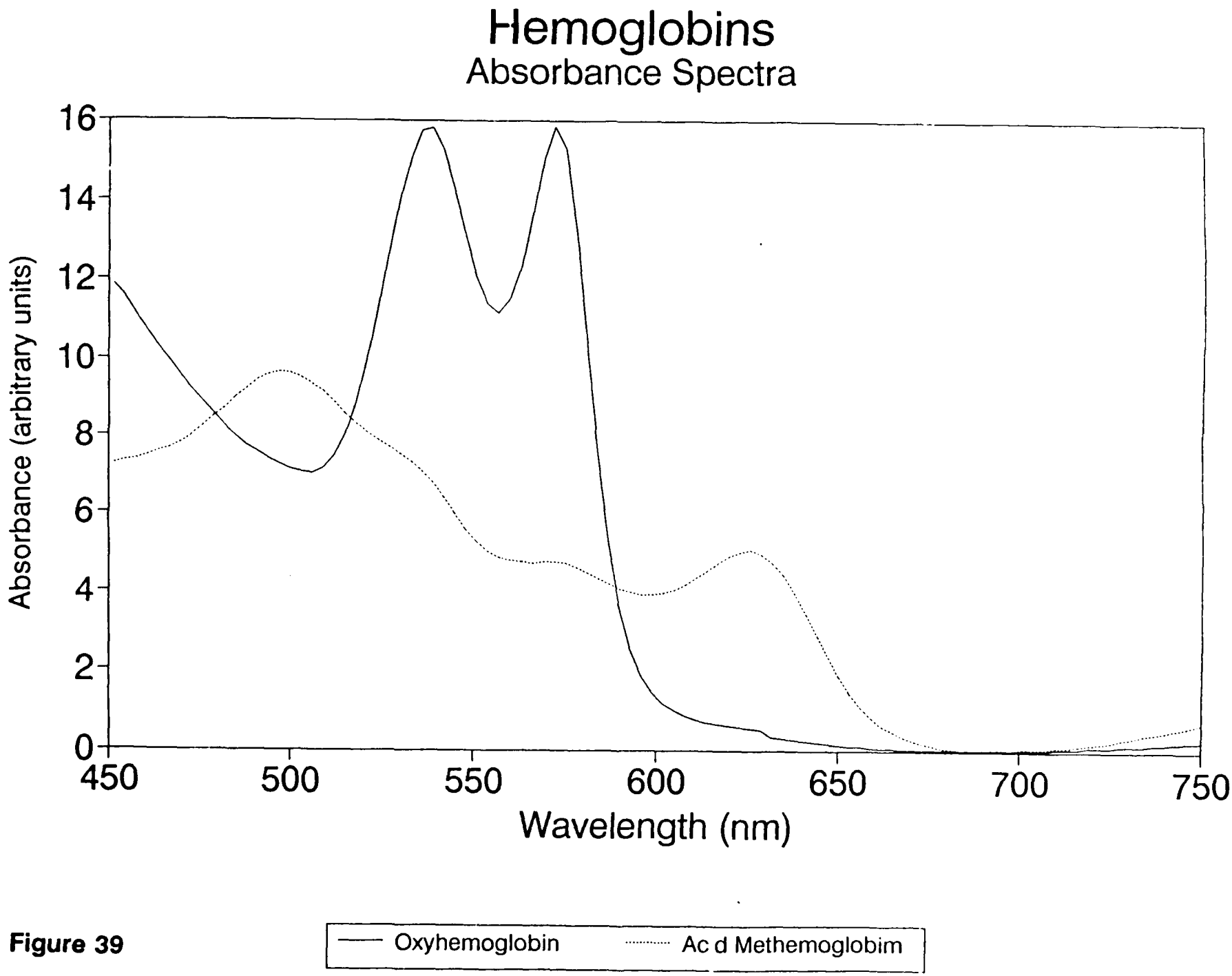
Hemoglobins
Absorbance Spectra
Absorbance (arbitrary units)
16
14
12
10
8
6
4
2
0
450
500
550
600
650
700
750
Wavelength (nm)
Oxyhemoglobin
Ac d Methemoglobim

Figure 39

R from PCA

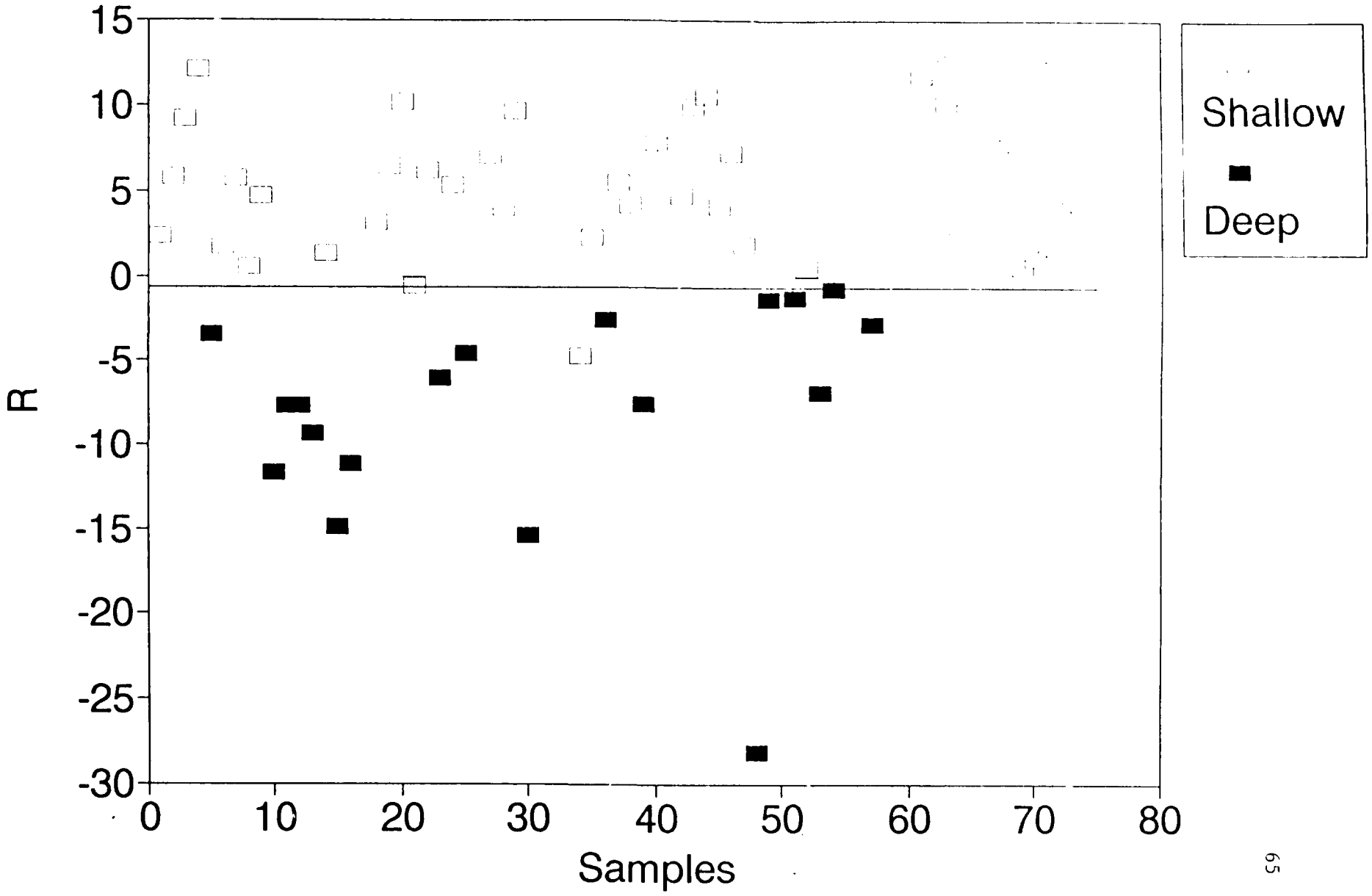

Figure 40

Curve Fitting
Basis Set

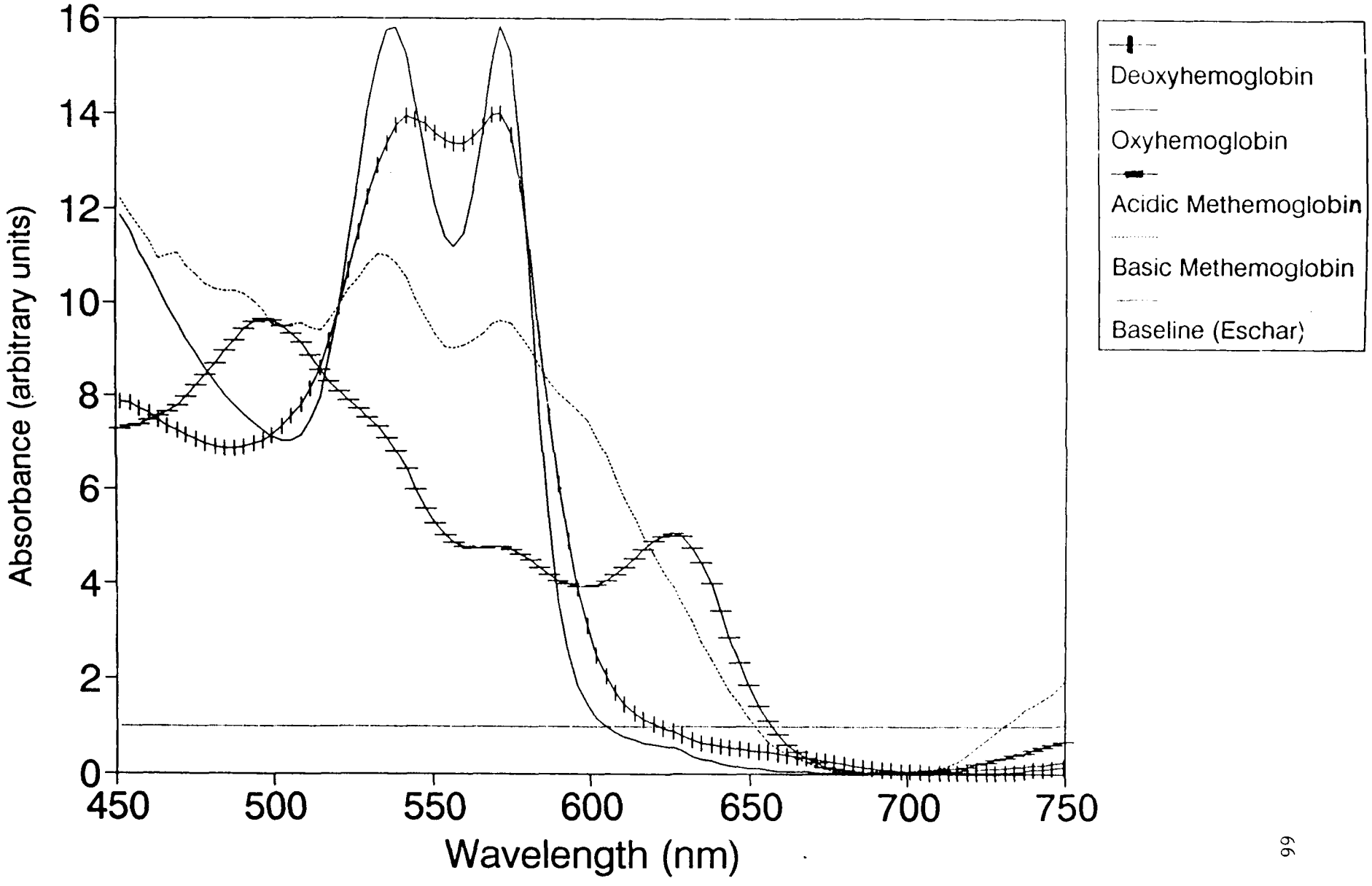

Figure 41

Curve Fitting Results

Shallow

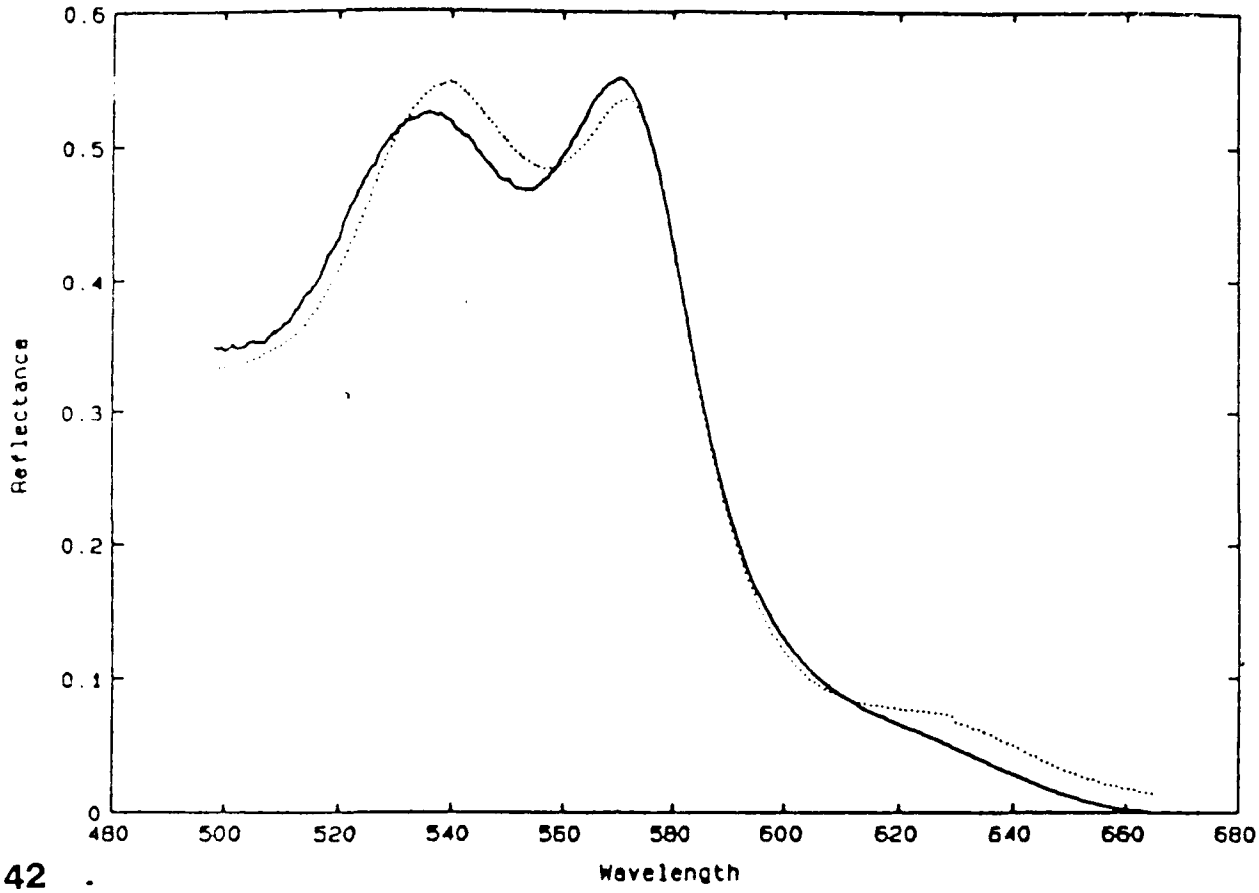

Figure 42

Deep

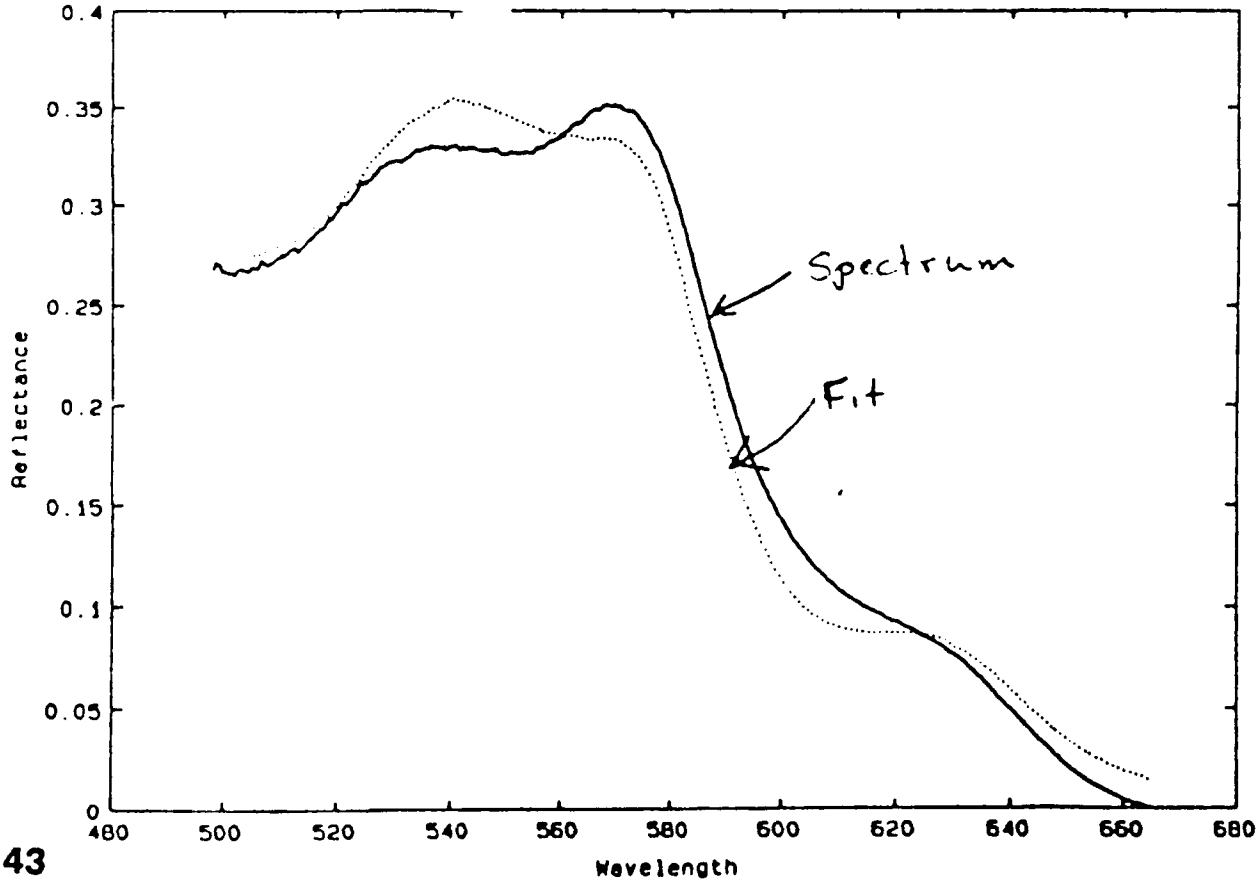

Figure 43

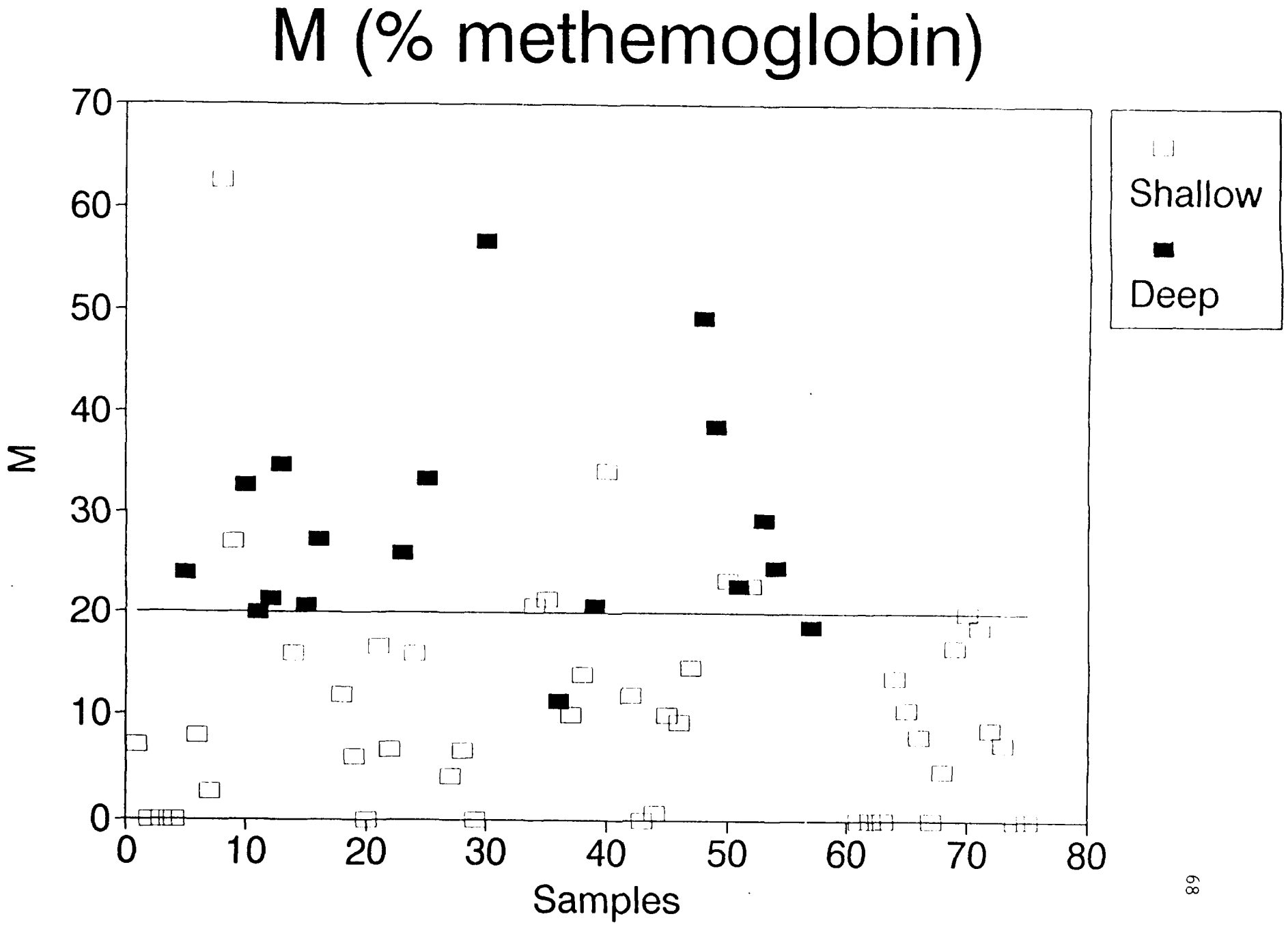
M (% methemoglobin)
M
70
60
50
40
30
20
10
0
0
10
20
30
40
50
60
70
80
Samples
Shallow
Deep

Figure 44